Contrib Mineral Petrol (2009) 158:505–527
DOI 10.1007/s00410-009-0394-5

ORIGINAL PAPER

Differentiation and crystallization conditions of basalts from the Kerguelen large igneous province: an experimental study

Marcus Freise · Francois Holtz · Marcus Nowak · James S. Scoates · Holger Strauss

Received: 17 April 2007 / Accepted: 23 February 2009 / Published online: 18 April 2009

Abstract Phase relations of basalts from the Kerguelen large igneous province have been investigated experimentally to understand the effect of temperature, fO_2, and fugacity of volatiles (e.g., H_2O and CO_2) on the differentiation path of LIP basalts. The starting rock samples were a tholeiitic basalt from the Northern Kerguelen Plateau (ODP Leg 183 Site 1140) and mildly alkalic basalt evolved from the Kerguelen Archipelago (Mt. Crozier on the Courbet Peninsula), representing different differentiation stages of basalts related to the Kerguelen mantle plume. The influence of temperature, water and oxygen fugacity on phase stability and composition was investigated at 500 MPa and all experiments were fluid-saturated. Crystallization experiments were performed at temperatures between 900 and 1,160°C under oxidizing (log $fO_2 \sim \Delta QFM + 4$) and reducing conditions (log $fO_2 \sim$ QFM) in an internally heated gas-pressure vessel equipped with a rapid quench device and a Pt-Membrane for monitoring the fH_2. In all experiments, a significant influence of the fO_2 on the composition and stability of the Mg/Fe-bearing mineral phases could be observed. Under reducing conditions, the residual melts follow a tholeiitic differentiation trend. In contrast, melts have high Mg# [$Mg^{2+}/(Mg^{2+} + Fe^{2+})$] and follow a calk-alkalic differentiation trend at oxidizing conditions. The comparison of the natural phenocryst assemblages with the experimental products allows us to constrain the differentiation and pre-eruptive conditions of these magmas. The pre-eruptive temperature of the alkalic basalt was about 950–1,050°C. The water content of the melt was below 2.5 wt% H_2O and strongly oxidizing conditions (log $fO_2 \sim \Delta QFM + 2$) were prevailing in the magma chamber prior to eruption. The temperature of the tholeiitic melt was above 1,060°C, with a water content below 2 wt% H_2O and a log $fO_2 \sim \Delta QFM + 1$. Early fractionation of clinopyroxene is a crucial step resulting in the generation of silica-poor and alkali-rich residual melts (e.g., alkali basalt). The enrichment of alkalis in residual melts is enhanced at high fO_2 and low aH_2O.

Keywords Large igneous provinces · Basalt · Oxygen fugacity · Liquid lines of descent · Phase relations · Crystallization experiments

Communicated by T. L. Grove.

Electronic supplementary material The online version of this article (doi:10.1007/s00410-009-0394-5) contains supplementary material, which is available to authorized users.

M. Freise (✉) · F. Holtz · H. Strauss
Institut für Mineralogie, Universität Hannover, Callinstr. 3, 30167 Hannover, Germany
e-mail: M.Freise@mineralogie.uni-hannover.de

M. Nowak
Institut für Geowissenschaften, Universität Tübingen, Wilhelmstr. 56, 72072 Tübingen, Germany

J. S. Scoates
Department of Earth and Ocean Sciences, University of British Columbia, 6339 Stores Road, Vancouver, BC V6T 1Z4, Canada

Introduction

The formation of large igneous provinces (LIPs) is related to periods of intense volcanic activity on the Earth's surface (e.g., Courtillot 1999). LIPs are constructed when large amounts of mantle-derived basaltic magma enter the Earth's crust in localized regions. The two most voluminous LIPs are Cretaceous oceanic plateaus, Ontong-Java in the Pacific Ocean (Korenaga 2005) and Kerguelen Plateau/Broken Ridge in the southern Indian Ocean (Coffin et al.

2002). LIPs such as Ontong Java and Kerguelen Plateau are related to hotspot magmatism and the origin, formation and differentiation of the generated magmas have been investigated with a variety of petrological and geochemical tools to constrain the possible magma sources, differentiation paths and the role of the important parameters controlling differentiation processes [e.g., pressure, temperature, oxygen fugacity (fO_2), phase stability, amount of volatiles]. Forward modeling of major element variations and of petrological processes is increasingly performed using empirical or thermodynamic models, which are calibrated on the results of experimental studies. Currently, the most popular thermodynamic models used to predict phase relations in basaltic systems are those developed by Ghiorso and Sack (1995) and Ariskin (1999). The experimental database for basaltic systems is mainly derived from MORB-like or tholeiitic anhydrous compositions. For basaltic systems, there is a notable lack of data at moderate to low pressures (<800 MPa) and hydrous conditions. Many basalt compositions, such as ferrobasalts or LIP basalts, can differ strongly from MORB compositions (e.g., in their Fe/Mg ratios and alkali contents), which in turn will influence the liquid lines of descent.

Experimental studies on LIP-related basalts have been mainly confined to 1 atm (e.g., Thy et al. 1998). These experiments show that fractional crystallization of Fe–Ti oxides during the late stage of differentiation of a tholeiitic LIP-magma can lead to the formation of SiO_2-rich melts and magmas. However, anhydrous experiments need to be extrapolated to volatile-bearing systems (e.g., H_2O, CO_2 and S) to simulate more geologically relevant conditions. Although volatiles may be present only in low concentrations, they are dissolved in melts at high pressure and can significantly influence phase relations. Experiments on hydrous MORB systems at higher pressure were performed by Holloway and Burnham (1972), Helz (1973), Helz (1976), Dixon-Spulber and Rutherford (1983), Ellis and Thompson (1986). Importantly, the influence of oxygen fugacity or the composition of the volatile species (C–H–O, C–H–O–S) was not investigated in these studies. Variations of up to three log-units in fO_2 are possible in basaltic systems (e.g., Danyushevsky and Sobolev 1996; Ablay et al. 1998). Some previous experiments on MORB compositions have also been conducted at H_2O-saturated conditions and pressures above 1 GPa. Such conditions are not necessarily relevant for natural systems because the early stages of differentiation occur at water-undersaturated conditions. Water contents of about 0.4–0.9 wt% are found in tholeiites from Hawaii (Dixon et al. 1991; Johnson et al. 1994), up to 1.5 wt% were detected in plume-influenced MORB (Dixon et al. 2002), and up to 0.7 wt% have been measured in submarine basaltic glasses from the northern Kerguelen Plateau (Wallace 2002). The results of Borisova et al. (2002) further indicate that higher water contents (up to 2 wt%) can be incorporated in glass inclusions from alkali rich compositions from the Kerguelen Plateau. In addition, high-pressure experiments on MORB compositions should not be used to interpret differentiation processes in LIP-related basalts; LIP basalts are more enriched in TiO_2, FeO* (total Fe expressed as FeO) and total alkalis. Although some of these compositional differences may be small, they may affect significantly differentiation processes.

In this study, the phase relations of two basalts from the Kerguelen LIP have been investigated at 500 MPa to quantify the influence of temperature, fO_2, and aH_2O on phase assemblages and phase compositions during differentiation of tholeiitic and mildly alkaline LIP-related basalts. The results are used to determine the possible pre-eruptive conditions of the investigated rock samples by comparing the experimental products with the natural phenocryst assemblage.

Geological setting

The 8,500 km^2 Kerguelen Archipelago is the emergent part of the Northern Kerguelen Plateau, which is part of the large submarine Kerguelen Plateau on the Antarctic plate in the Southern Indian Ocean (Fig. 1). Volcanic rocks related to the Kerguelen hotspot have been erupted since ~130 Ma (e.g., Duncan 2002; Coffin et al. 2002). The Kerguelen Archipelago is mainly composed of tholeiitic-transitional to mildly alkalic "flood basalts" that cover more than 85% of the surface and can be divided into older tholeiitic-transitional basalts (29–26 Ma) and younger mildly alkalic basalts (25–24 Ma) (Nicolaysen et al. 2000). Within the Southeast Province of the archipelago there are also numerous younger (10–6 Ma) basanite to phonolite flows, plugs and intrusions (Weis et al. 1993; Freise et al. 2003). The petrologic and geochemical characteristics of basaltic and differentiated rocks from the Kerguelen Plateau and Archipelago can be found in Weis et al. (1989), Gautier et al. (1990), Weis et al. (1993), Weis et al. (1998), Yang et al. (1998), Frey et al. (2000a), Frey et al. (2000b), Damasceno et al. (2002), Doucet et al. (2002), Weis et al. (2002), Weis and Frey (2002), Ingle et al. (2003) and Doucet et al. (2005).

Starting materials

One set of experiments was performed with a submarine tholeiitic basalt (~34 Ma) from the ODP Leg 183 Site 1140 (35R2-89-88, here referred to as 35R2), which was drilled on the Northern Kerguelen Plateau (Fig. 1; Weis and Frey 2002). The major element composition is given

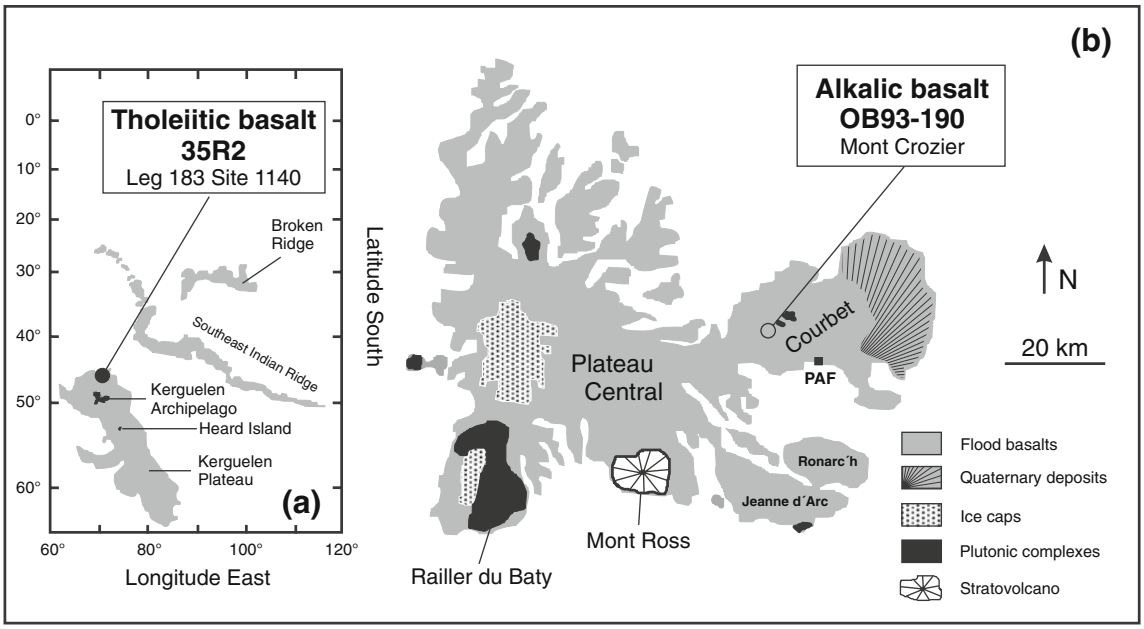

Fig. 1 Simplified map showing the location of the Kerguelen Archipelago in the Indian Ocean and the major geological units of the Kerguelen Archipelago modified after Damasceno et al. (2002). **a** Bathymetric map of a part of the Indian Ocean showing the major topographic features. **b** Geological map of the Kerguelen Archipelago. Also indicated are the sampling locations of both investigated basalts (35R2 and OB93-190)

Table 1 Starting compositions (wt%)

	Microprobe analysis of the starting glasses[a,b]				XRF analysis[b,c]		Microprobe analysis[a,b]	
	Alkali basalt OB93-190	1σ	Tholeiitic basalt 35R2	1σ	Alkali basalt OB93-190	Tholeiitic basalt 35R2	Alkali basalt KGL2	1σ
SiO_2	48.84	0.54	50.40	0.37	47.94	49.76	49.09	0.36
TiO_2	2.75	0.07	1.49	0.07	2.69	1.47	3.74	0.10
Al_2O_3	16.14	0.26	14.84	0.19	16.14	14.94	12.66	0.20
$Fe_2O_{3tot.}$	NA	NA	NA	NA	12.93	11.75	NA	NA
$FeO_{tot.}$	11.85	0.32	11.00	0.34	NA	NA	10.34	0.42
MnO	0.17	0.05	0.16	0.09	0.17	0.17	0.07	0.07
MgO	5.86	0.13	6.82	0.18	5.78	6.65	8.02	0.20
CaO	9.76	0.16	12.57	0.28	9.64	12.52	10.92	0.13
Na_2O	3.12	0.15	2.62	0.18	3.19	2.54	2.59	0.21
K_2O	1.12	0.07	0.09	0.03	1.16	0.10	2.20	0.10
P_2O_5	0.40	0.08	NA	NA	0.37	0.10	0.38	0.09
Total	100.00		100.00		100.00	100.00	100.00	
Total microprobe	99.32		99.56				99.23	

[a] Glass compositions are average values from 20 analyses for OB93 and 35R2, 30 analyses for KGL2

[b] All analyses are normalized to 100 wt%

[c] XRF analysis (anhydrous) from (D. Weis, personal communication)

[d] XRF analysis (anhydrous) from Weis and Frey (2002)

in Table 1. The microcrystalline sample contains phenocrysts of ~6 vol% plagioclase ($An_{83–70}$) and ~2 vol% clinopyroxene (Mg# = 85.8). A second set of experiments was performed with a basalt (~24 Ma) from the Mont Crozier section (OB93-190; Fig. 1) collected on the Courbet Peninsula of the Kerguelen Archipelago and mainly composed of mildly alkalic to alkali basalts (Damasceno et al. 2002). This more differentiated alkalic

basalt (Table 1), has lower SiO_2 and CaO contents and Mg# than the tholeiitic basalt 35R2, and higher total alkalis and TiO_2 contents than in 35R2. Sample OB93-190 contains phenocrysts consisting of ~4 vol% plagioclase ($An_{76–69}$), less than 0.5 vol% olivine (altered) and ~1 vol% clinopyroxene (Mg# = 75.6) in a microcrystalline groundmass (proportions determined using the software "Image Analysis©", e.g., Gardien et al. 1995; Koepke et al. 1996).

In addition to the two natural compositions OB93 and 35R2, a third synthetic composition (KGL2; Table 1) was prepared to perform kinetic experiments (see below). This composition is also an alkali basalt and is representative of basaltic glasses analyzed in inclusions in olivine phenocrysts collected from dredged rocks from the North Kerguelen Plateau (Borisova et al. 2002).

Experimental conditions and analytical techniques

Choice of experimental conditions

The experimental conditions chosen for this study are based on the pressure and temperature estimations determined for the mildly alkalic basalts of the Mont Crozier section from Damasceno et al. (2002). Clinopyroxene-liquid thermobarometry and clinopyroxene structural barometry on the Mont Crozier lavas indicate that magmas stalled and fractionated near the crust–mantle interface, which is estimated to be at 600 ± 100 MPa. Therefore, important differentiation processes involved in the evolution of the mildly alkalic basalts of the Kerguelen Archipelago are expected to occur in this pressure range. All experiments were performed in the temperature range 900–1,160°C and at 500 MPa, which is the pressure limit of the internally heated pressure vessel used for this study. Considering that no systematic database is available for modeling fractionation processes in basaltic systems relevant to the Kerguelen LIPs, we performed an experimental study to generate a set of data over a broad range of water activity and oxygen fugacity. Melt H_2O contents were varied from about 9 wt% (H_2O-saturated conditions at 500 MPa) down to 1 wt% in the most H_2O-undersaturated runs. The prevailing fO_2 in Kerguelen magmas has not been fully constrained. The fO_2 range adopted in this study (QFM and ΔQFM + 4) was guided by investigations of Ballhaus (1993), Borisova et al. (2002) and Ryabchikov et al. (2002). In this study, QFM and ΔQFM + 4 represent the fO_2 at quartz–fayalite–magnetite buffer conditions and intrinsic conditions, respectively. Borisova et al. (2002) suggested reducing conditions of around log fO_2 ~ QFM for the formation of picritic basalts on seamounts south of the Kerguelen Archipelago, whereas Ballhaus (1993) and Ryabchikov et al. (2002) observed more oxidizing conditions (log fO_2 ~ ΔQFM + 3) for OIB and LIP settings.

Starting materials for experiments and preparation of charges

Preparation and pre-equilibration of starting glass

The natural samples were first ground in a ball-mill to ~100 μm, loaded in a Pt crucible and fused twice (with regrinding in between) for 1 h at 1,600°C and 1 atm (in air) to a homogeneous, crystal-free and dry glass. The major element compositions of the obtained glasses were determined by electron microprobe (EMP) and are given in Table 1. The compositions of the natural rock and of the synthesized glass are identical within error. For crystallization experiments at oxidizing conditions (log fO_2 ~ QFM + 4), the glass powder synthesized at 1 atm was directly placed in noble capsules. For crystallization experiments at reducing conditions (log fO_2 ~ QFM), the oxidation state of iron (Fe^{2+}/Fe^{3+}) in the glass powder was pre-equilibrated in a gas-mixing furnace (H_2/H_2O) at 1 atm [Method described in Nafziger et al. (1971)]. The glass powder was placed in a ceramic crucible 40 mm in diameter and melted at 1,250°C for 120 min at QFM. This duration should be sufficient to equilibrate the Fe^{2+}/Fe^{3+} in the melt (Gaillard et al. 2002). Subsequent EMP analysis showed a contamination of Al at the rim of the glass cylinder (2–3 mm). Therefore, the uncontaminated central part was drilled out with a core driller.

Pre-saturation of capsule material

The experiments were performed using $Au_{80}Pd_{20}$ capsules with a 3.2 mm outer diameter, 0.2 mm wall thickness and 15 mm in length. Pt capsules are typically used to conduct high temperature experiments. However, iron is highly soluble in Pt-metal at high temperatures. To avoid iron loss, $Au_{80}Pd_{20}$ capsules with a melting point of 1,360°C at 500 MPa were used (e.g., Ford 1978; Ratajeski and Sisson 1999). In this alloy, under oxidizing conditions, Fe is less soluble in $Au_{80}Pd_{20}$ than in Pt and no significant iron loss is observed after the experiments (Berndt et al. 2005). For experiments under reducing conditions (log fO_2 < ΔQFM + 4), the $Au_{80}Pd_{20}$ capsules were pre-saturated with iron to minimize iron loss from the melt, using the experimental approach and a MORB composition described by Berndt et al. (2005). Capsules were equilibrated in an 1 atm gas-mixing furnace in a synthetic basaltic melt with a bulk composition similar to OB93-190 at 1,250°C and log fO_2 ~ QFM for 3 days.

After equilibration and quenching, the capsules were extracted from the surrounding glass by placing them in hydrofluoric acid.

Preparation of charges

Capsules were cleaned in acetone and annealed for 1 h at 1,000°C at 1 atm. The capsules were first welded shut at one end with an electric arc and filled with H_2O, $Ag_2C_2O_4$ (used as CO_2 source) and glass powder crushed to a grain sizes of <150 μm. A small grain size is necessary to reach equilibrium conditions within short run duration, because the volatiles have to diffuse from the fluid phase into the dry glass fragments at the beginning of the experiment.

The filled capsules were cooled in liquid nitrogen and welded shut. The closed capsules were subsequently heated in a drying furnace for 120 min at 200°C to decompose the $Ag_2C_2O_4$ to Ag and CO_2, and to test for possible leakage. The purity of $Ag_2C_2O_4$ was tested using the gravimetric determination of Bohlen et al. (1982). The observed weight loss was 93% of the expected value. The molar ratio of H_2O (XH_2O) in the fluid phase was varied with different H_2O–CO_2 mixtures. In all experiments the initial amount of fluid was 12 wt%.

Experimental equipment and run procedure

All crystallization experiments were conducted in an internally heated pressure vessel (IHPV) with either Ar (log $fO_2 \sim$ QFM + 4 at water-saturated conditions) or Ar–H_2 (log $fO_2 \sim$ QFM at water-saturated conditions) mixtures as a pressure medium. The sample holder was equipped with a rapid-quench device (e.g., Roux and Lefèvre 1992) and a Pt-membrane for monitoring the H_2 fugacity during the entire experiment (Scaillet et al. 1995; Berndt et al. 2002). The temperature in the IHPV was recorded by two S-type thermocouples with an uncertainty of ±3°C. Each experiment consisted of a set of four capsules which were heated at 30°C/min to run temperature. The run duration was about 24 h for oxidizing conditions and 3–6 h for reducing conditions to minimize changes in melt FeO content due to alloying with the capsule material. After quenching, each capsule was punctured and weighed to check for the presence of a fluid phase.

Calculation of aH_2O, fH_2O and fO_2

The phase equilibria experiments conducted in this study are fluid-saturated. However, the amount of free fluid phase was low (to avoid incongruent dissolution of the silicate in the fluid phase) and the concentrations of H_2O and CO_2 in the fluid phase could not be determined accurately in the experimental products. Thus, the H_2O activity (aH_2O) in each experiment was calculated using the solubility model of Burnham (1979) which requires the determination of the water concentration in the quenched glass. However, Holtz et al. (1995) demonstrated that the model of Burnham significantly underestimates H_2O solubility at high pressures. Thus, we applied a correction factor to the aH_2O calculated after the model of Burnham (1979) for each set of experiments at a given temperature (maximum correction is 20% relative). This factor corresponds to the ratio between aH_2O at water saturated conditions ($aH_2O = 1.0$) and the aH_2O calculated following the model Burnham (1979) for the melt water content determined at water saturated conditions (Tables 2, 3, 4).

The calculation of the prevailing fO_2 in the experiments can be performed using the dissociation reaction of water (there is a free fluid phase in the experiments) if the H_2O fugacity (fH_2O) and H_2 fugacity (fH_2) are known (e.g., Scaillet et al. 1995). The fH_2O was calculated with following equation:

$$fH_2O = aH_2O \cdot f^0H_2O \quad (1)$$

f^0H_2O data were taken from Pitzer and Sterner (1994). Knowing fH_2O and fH_2 (measured PH_2 multiplied by the H_2 fugacity coefficients of Shaw and Wones (1964), fO_2 can be recalculated at a given pressure and temperature. The fH_2O decreases with XH_2O and the equilibrium constant of the dissociation reaction of H_2O shows that decreasing fH_2O causes a decrease in fO_2 (Scaillet et al. 1995). At known fH_2O and fH_2, the fO_2 can be calculated following Eq. 2:

$$K_W = \frac{fH_2O}{fH_2 \cdot \sqrt{fO_2}} \quad (2)$$

The dissociation constant K_W of H_2O was taken from Robie et al. (1978). For each experiment, fO_2 was calculated depending on the water content in the melt. As the experiments were conducted either at oxidized or at reduced conditions, with a variation of nearly four log units for experiments performed at identical temperature and aH_2O, the datasets obtained at reduced conditions will be labeled as ~QFM and those obtained at oxidizing conditions will be labeled as ~ΔQFM + 4 in the following discussion. The quantity ΔQFM is the difference between the natural logarithm of fO_2 of the experiments and the log fO_2 of the quartz–fayalite–magnetite buffer determined by Schwab and Küstner (1981).

Analytical techniques

The compositions of the natural minerals and all run products were characterized by EMP and scanning electron microscopy (SEM). The major elements of the starting

Table 2 Experimental conditions, run products and phase proportions for the tholeiitic basalt (35R2) at ΔQFM + 4

Run	Run duration [h]	XH_2O_{in}[a]	H_2O [wt%][b]	aH_2O	fH_2O [bar]	log fO_2 [bar][c]	ΔQFM [bar][d]	Run products
960°C, 500 MPa								
126	22	1.00	9.48	1.00	5,524	−7.17	+4.00	gl (41.8), mag (10.5), cpx (43.2), am (4.5), s^2 (0.72)
127	22	0.79	7.82	0.80	4,396	−7.37	+3.80	gl (32.0), mag (9.6), cpx (46.3), am (6.3), pl (5.8), s^2 (0.64)
1,000°C, 500 Mpa								
108	22	1.00	9.59	1.00	5,706	−6.55	+4.00	gl (50.0), mag (9.6), cpx (40.4), s^2 (0.82)
109	22	0.81	7.74	0.81	4,622	−6.73	+3.82	gl (45.5), mag (9.1), cpx (44.0), pl (1.3), s^2 (0.48)
110	22	0.61	3.52	0.37	2,105	−7.41	+3.13	gl (34.9), mag (9.2), cpx (47.3), pl (7.4), ilm (1.2), s^2 (0.51)
111	22	0.41	ND	ND	ND	ND	ND	mag (10.1), cpx (62.7), pl[e] (22.8), ilm (4.4)
1,040°C, 500 Mpa								
112	24	1.00	9.67	1.00	5,869	−5.96	+4.00	gl (89.8), mag (3.8), cpx (6.3), s^2 (0.10)
113	24	0.80	5.83	0.53	3,108	−6.51	+3.45	gl (73.8), mag (4.6), cpx (21.6), s^2 (0.14)
114	24	0.60	4.44	0.39	2,266	−6.79	+3.17	gl (61.8), mag (6.7), cpx (30.6), ilm (0.9), s^2 (0.29)
115	24	0.42	0.62	0.02	92	−9.57	+0.39	gl (50.1), mag (8.1), cpx (34.3), pl[e] (5.8), ilm (1.7)
1,080°C, 500 MPa								
116	23	1.00	9.55	1.00	6,014	−5.41	+4.00	gl (98.0), mag (2.0), s^2 (0.04)
117	23	0.78	7.58	0.74	4,426	−5.67	+3.73	gl (88.6), mag (3.3), cpx (8.1), s^2 (0.11)
118	23	0.58	2.11	0.13	811	−7.15	+2.26	gl (72.7), mag (3.9), cpx (23.4), s^2 (0.04)
119	23	0.39	1.17	0.06	348	−7.88	+1.52	gl (47.2), mag (5.7), cpx (30.8), pl 16.3), s^2 (0.07)
1,120°C, 500 MPa								
120	23	1.00	9.27	1.00	6,142	−4.88	+4.00	gl (100)
121	23	0.78	6.01	0.65	3,986	−5.26	+3.62	gl (98.8), mag (1.2), s^2 (0.54)
122	23	0.60	2.95	0.29	1,798	−5.95	+2.93	gl (88.5), mag[e] (1.0), cpx[e] (10.5)
123	23	0.36	0.46	0.01	73	−8.74	+0.15	gl (75.3), mag (0.7), cpx (19.3), pl (4.7), s^2 (0.01)
1,160°C, 500 MPa								
124	22	0.58	4.22	0.46	2,859	−5.07	+3.32	gl (99.8), mag (0.2), s^2 (0.05)
125	22	0.41	3.12	0.32	1,986	−5.39	+3.00	gl (98.3), mag (0.2), cpx (1.5), s^2 (0.10)
1,250°C, 500 MPa								
S1	25	–	4.45	0.49	3,158	−4.00	+3.38	gl (100)
S2	25	–	2.08	0.18	1,616	−4.85	+2.53	gl (100)

s^2 is the residual of the mass balance calculation, when s^2 value is not given, the proportions were calculated on the basis of image analysis and should be considered as rough estimates

gl glass, *mag* magnetite, *ilm* ilmenite, *cpx* clinopyroxene, *am* amphibole, *pl* plagioclase, *ol* olivine

[a] $XH_2O_{in} = H_2O/(H_2O + CO_2)$ loaded in capsule (in mole fraction)

[b] H_2O content of the glasses determined using the "by-difference" method

[c] log fO_2 was calculated considering that the intrinsic buffering capacity of the used IHPV is on the MnO–Mn_3O_4 buffer curve (for further explanation, see text)

[d] ΔQFM indicates log fO_2 (experiment) − log fO_2 (QFM buffer) as estimated by Schwab and Küstner (1981)

[e] Phases have been identified qualitatively

glasses and experimental phases were analyzed with a Cameca Camebax MB and SX100. The data for the crystalline phases and glasses were acquired with an accelerating voltage of 15 kV/15 nA and 15 kV/4 nA, respectively. Counting times for Na and K were 5 s for minerals and 2 s for glasses. For the other elements, the counting times were 10 s for minerals and 5 s for glasses. For glasses, the beam size was defocused to 10–20 μm, depending on the crystal content of the samples to minimize the migration of alkalis (Hunt and Hill 2001). Freise et al. (2003) showed that no correction for alkali loss is necessary with this analytical procedure. The H_2O concentrations of the glasses were determined using the EMP and the "by-difference" method (e.g., Devine et al. 1995; Koepke 1997; Berndt 2002; Freise et al. 2003; Berndt et al. 2005). To check the reliability of this method, the results of

Table 3 Experimental conditions, run products and phase proportions for the tholeiitic basalt (35R2) at QFM

Run	Run Duration [h]	XH_2O_{in}a	H_2O [wt%][b]	aH_2O	fH_2O [bar]	log fO_2 [bar][c]	ΔQFM [bar][d]	Run products[e]
1,000°C, 495.3 MPa								
128	5.2	1.00	9.11	1.00	5,629	−10.55	±0.00	gl (83.0), cpx (17.0), s^2 (0.41)
129	5.2	0.79	6.40	0.64	3,617	−10.93	−0.38	gl (70.7), cpx (27.0), am (2.3), s^2 (0.47)
130	5.2	0.61	5.08	0.52	2,924	−11.12	−0.56	gl (56.5), cpx (30.4), am (8.0), pl (3.9), ol (1.2), s^2 (0.29)
131	5.2	0.44	3.45	0.35	1,949	−11.47	−0.92	gl (29.1), cpx (38.8), am (3.6), pl (25.6), ol (2.2), ilm (0.6), s^2 (0.35)
1,040°C, 499.6 MPa								
132	3.5	1.00	9.18	1.00	5,862	−9.96	±0.00	gl (94.8), cpx (5.2), s^2 (0.19)
133	3.5	0.81	6.01	0.59	3,452	−10.42	−0.45	gl (84.1), cpx (15.9), s^2 (0.35)
134	3.5	0.60	4.80	0.43	2,506	−10.69	−0.73	gl (77.1), cpx (15.9), s^2 (0.29)
135	3.5	0.43	2.28	0.16	959	−11.53	−1.57	gl (62.4), cpx (30.8), pl (6.8), s^2 (0.42)
1,080°C, 515.2 MPa								
136	3.2	1.00	9.29	1.00	6,279	−9.39	±0.00	gl (100)
137	3.2	0.79	5.63	0.57	3,584	−9.88	−0.48	gl (94.6), cpx (5.4), s^2 (0.34)
138	3.2	0.60	4.32	0.39	2,419	−10.22	−0.82	gl (83.4), cpx (16.6), s^2 (0.33)
139	3.2	0.42	3.16	0.25	1,550	−10.61	−1.21	gl (80.7), cpx (19.3), s^2 (0.51)

For abbreviations, see Table 2

the "by-difference" method were compared with IR-measurements on the experimental glasses obtained from hyperliquidus run products. Linear absorbances of bands at 5,200 and 4,500 cm^{-1} (assigned to molecular H_2O and OH, respectively) were determined using a linear background correction for each peak. The H_2O concentrations were calculated using the absorption coefficients of the 5,200 and 4,500 cm^{-1} bands determined for basaltic glasses by Ohlhorst et al. (2001) and the Lambert Beer's Law. The H_2O contents determined by IR and "by-difference" method are identical within error (the maximal variation is 6.5% relative for glasses containing 2–10 wt% H_2O (see eTable 1). For a series of experiments, the water contents determined "by-difference" was overestimated because of technical problems with the microprobe (eight glasses, composition OB93-190; Table 5). For these experiments the water contents were calculated based on the amount of glass in the experimental product, the XH_2O initial and the solubility of mixed volatiles in an alkali-rich andesitic melt (Botcharnikov et al. 2006; the residual melts in these experiments are closer to andesite than to basalt).

The phase proportions were calculated using the mass balance method given by Albarède (1995). The low residuals show that the glasses (normalized to 100 wt%) were correctly analyzed and that no major phase was missing in the calculations (see values of s^2 systematically lower than 1 in Tables 2, 3, 4). In some experiments, mostly experiments with low glass proportions, the residuals were estimated to be too high ($s^2 > 1$) and quantitative phase analyses were missing. The residuals may be higher in experiments with low melt fraction because some accessory phases, expected to be present, were not taken into account (e.g., apatite). For these runs, phase proportions were determined with SEM pictures and the software "Image Analysis©" (e.g., Gardien et al. 1995; Koepke et al. 1996). However, the uncertainty with this technique is high when compared to the mass balance method and the phase proportions should be considered as rough estimations.

Experimental results

General observations

The experimental products consist of mixtures of glass, crystals and fluid (Tables 2, 3, 4; eTables 2, 3). In all experiments the crystals and fluid phase (bubbles filled with H_2O only or mixtures of H_2O and CO_2) were homogeneously distributed throughout the sample. Figure 2 shows SEM images from typical experimental products of the mildly alkalic basalt (OB93-190) at H_2O-saturated and oxidizing conditions (log $fO_2 \sim$ ΔQFM + 4) between 900 and 1,100°C. Crystal lengths were mostly between 8 and 15 μm, except for some amphibole and olivine crystals, which reached lengths of 20 μm (olivine) and 30 μm (amphibole) or more. Different observations indicate that near-equilibrium conditions prevailed during the experiments: (1) the crystals are distributed homogeneously in the glass matrix in all experiments, (2) the chemical

Table 4 Experimental conditions, run products and phase proportions for the alkali basalt (OB93-190) at ΔQFM + 4

Run	Run duration [h]	XH_2O_{in}[a]	H_2O [wt%][b]	aH_2O	fH_2O [bar]	log fO_2 [bar][c]	ΔQFM [bar][d]	Run products[e]
900°C, 500 MPa								
60	22	1.00	9.19	1.00	5,214	−8.19	+4.00	gl (48.0), mag[e] (2.3), ilm (9.2), cpx (8.5), am (29.2), pl (5.1)
61	22	0.82	5.36	0.64	3,331	−8.58	+3.61	gl (13.1), mag[e] (4.2), ilm (8.8), cpx (14.6), am (38.7), pl (20.6)
950°C, 500 MPa								
54	22	1.00	9.19	1.00	5,476	−7.34	+4.00	gl (60.9), mag[e],(1.9), ilm (9.4), cpx (7.9), am (19.9)
55	22	0.81	6.56	0.53	2,914	−7.89	+3.45	gl (42.0), mag[e] (3.8), ilm (9.5), cpx (10.9), am (22.5), pl (11.3)
56	22	0.62	3.42	0.28	1,520	−8.45	+2.89	gl (16.0), mag (8.2), ilm[e] (9.8), cpx[e] (16.4), am (28.9), pl (20.7)
59	24	0.44	2.20	0.10	574	−9.29	+2.04	gl (10.1), mag (7.8), ilm[e] (9.2), cpx (20.1), am (30.2), pl (22.6)
1,000°C, 500 Mpa								
51	20	1.00	9.31	1.00	5,706	−6.55	+4.00	gl (80.5), mag (2.9), ilm (6.8), cpx (9.8), s^2 (0.59)
52	20	0.81	5.76	0.57	3,231	−7.04	+3.51	gl (68.4), mag (2.9), ilm (5.9), cpx (14.0), am (8.7), s^2 (0.42)
53	20	0.62	2.52	0.19	1,112	−7.97	+2.58	gl (43.6), mag (2.6), ilm (6.9), cpx (18.8), am (2.6), pl (6.9), ol (18.8), s^2 (0.82)
58	20	0.44	1.96	0.12	711	−8.36	+2.19	gl (33.7), mag (4.6), ilm (6.9), cpx (27.4), ol[e] (19.3), pl (8.1)
1,050°C, 500 MPa								
48	20	1.00	9.52	1.00	5,907	−5.82	+4.00	gl (95.6), mag (4.4), s^2 (0.45)
49	20	0.82	6.24	0.64	3,804	−6.20	+3.62	gl (95.5), mag (4.5), s^2 (0.11)
50	20	0.62	3.05	0.22	1,310	−7.13	+2.69	gl (74.9), mag (5.7), ilm (2.6), cpx (16.8), s^2 (0.50)
57	22	0.42	1.32	0.06	380	−8.20	+1.62	gl (68.6), mag (6.6), ilm (9.1), cpx (21.7), s^2 (0.61)
1,100°C, 500 MPa								
62	22	0.63	3.51	0.40	2,407	−5.95	+3.20	gl (94.7), mag (5.3), s^2 (0.09)
63	22	0.44	2.61	0.24	1,471	−6.38	+2.77	gl (84.4), mag (6.2), cpx (9.3), s^2 (0.07)
1,150°C, 500 MPa								
148	23	1.00	9.54	1.00	6,229	−4.52	+4.00	gl (100)
149	23	0.80	6.47	0.66	4,105	−4.88	+3.64	gl (99.4), mag (0.6), s^2 (0.07)
150	23	0.60	3.39	0.32	1,971	−5.51	+3.00	gl (99.5), mag (0.5), s^2 (0.19)
151	23	0.40	2.51	0.21	1,314	−5.87	+2.65	gl (99.4), mag (0.6), s^2 (0.11)

gl glass, *mag* magnetite, *ilm* ilmenite, *cpx* clinopyroxene, *am* amphibole, *pl* plagioclase, *ol* olivine

[a] $XH_2O_{in} = H_2O/H_2O + CO_2$ loaded in capsule (in mole fraction)

[b] H_2O content of the glasses determined using the "by-difference" method

[c] log fO_2 was calculated considering that the intrinsic buffering capacity of the used IHPV is on the MnO–Mn_3O_4 buffer curve (for further explanation, see text)

[d] ΔQFM indicates log fO_2 (experiment) − log fO_2 (QFM buffer) as estimated by Schwab and Küstner (1981)

[e] Phases have been identified qualitatively

composition of the synthesized phases changes systematically with the experimental conditions following expected trends (e.g., evolution of An content of plagioclases with changing temperature and aH_2O). Run duration was 20–25 h at log $fO_2 \sim$ ΔQFM + 4 and 3–6 h at log $fO_2 \sim$ QFM. Because of problems related to Fe-loss to the capsule material, the duration of experiments at reducing conditions was never longer than 6 h and the attainment of near equilibrium conditions need to be checked for these runs. A systematic change of experimental duration was not performed with the two investigated compositions. However, experiments with different run duration were carried out with a similar alkali-rich basaltic composition KGL2 (Table 1) and the results indicate that near-equilibrium conditions can be attained within 3 h (Table 1).

The pre-treatment of the starting melts at appropriate redox conditions is an additional factor in rapidly reaching near-equilibrium conditions. The starting basaltic glasses were placed in a furnace at redox conditions corresponding to those of the redox conditions of the crystallization experiments (at $aH_2O = 1.0$). At reducing conditions, despite the pre-saturated noble capsules, a relative Fe-loss

Table 5 Experimental conditions, run products and phase proportions for the alkali basalt (OB93-190) at QFM

Run	Run duration [h]	XH_2O_{in}a	H_2O [wt%][b]	aH_2O	fH_2O [bar]	log fO_2 [bar][c]	ΔQFM [bar][d]	Run products[e]
960°C, 500.3 MPa								
97	6	1.00	9.32	1.00	5,529	−11.17	±0.00	gl (71.2), am (27.7), ilm (1.1), s^2 (0.41)
98	6	0.81	6.93[b]	0.73	4013	−11.45	−0.27	gl (59.0), am (40.3), ilm (0.7), s^2 (0.57)
99	6	0.62	3.82	0.37	2,065	−12.03	−0.85	gl (20.2), am (49.5), ilm (1.1), cpx[f],(18.3) pl (10.9)
100	6	0.44	2.40	0.17	936	−12.71	−1.54	gl (10.7), am (44.4), ilm[f],,(2.5), cpx (21.9), pl[f],(16.2); ol (4.3)
1,000°C, 492.9 Mpa								
96	5	1.00	9.18	1.00	5,590	−10.55	±0.00	gl (97.4), ol (2.6), s^2 (0.33)
85	6	0.82	6.75	0.68	3,803	−10.88	−0.33	gl (67.3), am (32.4), ilm (0.3), s^2 (0.79)
86	6	0.62	5.03[b]	0.46	2,567	−11.23	−0.67	gl (58.2), cpx (6.5), am (30.2), ilm[f],(0.9), pl (4.2)
87	6	0.44	4.10[b]	0.37	2,057	−11.41	−0.86	gl (49.6), ol (1.3), cpx (14.9), am (24.5), ilm[f] (1.1), pl (8.6)
101	5	0.32	3.92[b]	0.36	2,013	−11.44	−0.88	gl (15.6), ol (1.7), cpx (28.5), am (31.9), ilm (3.1), pl (19.2)
102	5	0.22	2.04[b]	0.14	793	−12.25	−1.69	gl (13.3), ol (3.4), cpx (20.5), am (38.8), ilm[f] (4.3), pl (19.7)
1,040°C, 489.3 MPa								
80	4	1.00	9.28	1.00	5,690	−9.96	+0.00	gl (100)
81	4	0.82	7.30	0.76	4,336	−10.20	−0.23	gl (98.5), ol (1.5), s^2 (0.38)
82	4	0.63	4.32	0.41	2,329	−10.74	−0.77	gl (91.0), ol (0.6), cpx (8.4), s^2 (0.22)
83	4	0.42	2.84[b]	0.22	1,265	−11.27	−1.30	gl (72.9), ol (0.8), cpx (17.4), am (5.8), ilm[f] (0.9), pl (2.2)
103	3	0.31	1.65	0.10	580	−11.95	−1.98	gl (57.5), ol (7.1), cpx (14.6), ilm (2.2), pl (18.7), s^2 (0.37)
104	3	0.22	0.92	0.04	225	−12.77	−2.80	gl (52.9), ol (7.5), cpx (15.5), ilm (2.0), pl (22.1), s^2 (0.22)
1,080°C, 498.5 MPa								
88	3	1.00	9.27	1.00	5,988	−9.40	0.00	gl (100)
89	3	0.81	7.75	0.83	4,988	−9.56	−0.15	gl (100)
90	3	0.64	4.82[b]	0.50	2,970	−10.01	−0.60	gl (100)
91	3	0.40	2.91[b]	0.25	1,515	−10.60	−1.19	gl (88.5), ol (3.5), cpx (8.0)
1,120°C, 513.0 MPa								
92	3	1.00	9.40	1.00	6,374	−8.87	0.00	gl (100)
93	3	0.81	6.36[a]	0.65	4,171	−9.24	−0.36	gl (100)
94	3	0.62	4.79[a]	0.49	3,119	−9.49	−0.61	gl (100)
95	3	0.43	2.21[a]	0.17	1,090	−10.41	−1.53	gl (100)

For abbreviations, see Table 2

[a] Water content determined by IR measurements because of technical problems during the microprobe analytical session

[b] The water contents in the melts were corrected using the solubility data of mixed volatiles because of technical problems during the microprobe analytical session (see text)

of ~4 wt% FeO in the glass between core and rim of the sample was observed in runs at high temperature ($T > 1{,}100$°C). However, microprobe analyses show that the Fe-content of the glass in the middle of the sample is nearly constant and decreases only in the rim directly in contact with the capsule wall.

Kinetic experiments with the alkali basalt KGL2

The experiments were conducted at 1,100°C, 400 MPa, for $XH_2O = 0$ and $XH_2O = 0.2$ and the duration was 1 min (0.017 h) to 24 h (Table 6). For experiments with $XH_2O = 0$, no fluid phase was added to the starting dry glass. These strongly water-undersaturated conditions were chosen because kinetic problems related to nucleation and crystal growth may be expected mainly at low H_2O activities, considering that dry melts are more polymerized than hydrous melts. The results (Table 6) show that the glasses of the experimental products in the nominally dry experiments ($XH_2O = 0$) contain a non-negligible amount of water, as indicated by the estimation of the water content using the "by-difference method". This is related to the diffusion of H_2 through the noble metal capsule at high temperature (H_2 is present in small proportions in the gas medium). This also explains why the phase proportions observed in the two series of experiments do not differ strongly.

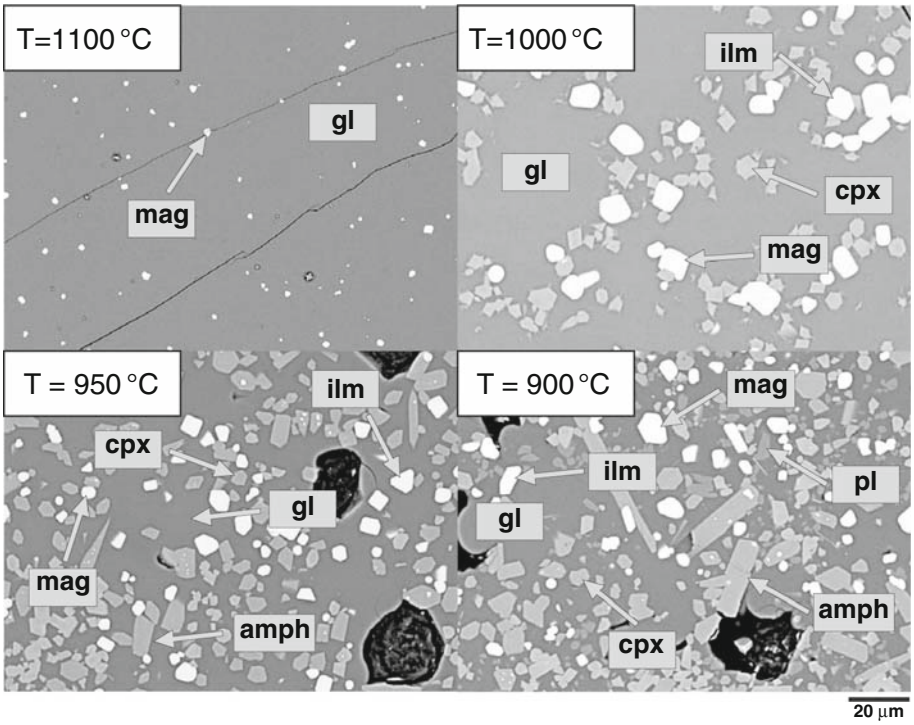

Fig. 2 Scanning electron microscope images of selected run products from crystallization experiments of the alkalic basalt (OB93-190) under oxidizing conditions (log $fO_2 \sim \Delta QFM + 4$) and $XH_2O = 1.0$ for different temperatures. *gl* glass, *mag* magnetite, *cpx* clinopyroxene, *ilm* ilmenite, *amph* amphibole, *pl* plagioclase

Table 6 Experimental conditions, run products and phase proportions for the alkali basalt KGL2 at ΔQFM + 4, 1,100°C and 400 MPa

Run	Run duration [h]	XH_2O_{in}a	H_2O [wt%][b]	aH_2O	fH_2O [bar][c]	log fO_2 [bar][c]	ΔQFM [bar][c]	Run products[d]
K45	0.017	0	–	–	–	–	–	–
K52	0.3	0	–	–	–	–	–	–
K49	1.7	0	1.4	0.11	474	−7.16	2.05	gl, plag, ol, cpx, mag
K39	3.0	0	1.8	0.15	669	−6.86	2.35	gl (57), plag (3.5), ol (<1), cpx (37), mag (<1), ilm (2.4)
K55	6.1	0	1.0	0.06	261	−7.68	1.35	gl (58), plag (3.4), ol (<1), cpx (35.9), mag (<1), ilm (2.3)
K42	17.7	0	1.2	0.07	335	−7.46	1.75	gl (55), plag (3.6), ol (<1), cpx (37.1), mag (1.1), ilm (2.8)
K33	24.0	0	2.0	0.18	784	−6.72	2.49	gl (63), plag (<1), ol (<1), cpx (34.4), mag (<1), ilm (1.8)
K73	24+	0	2.1	0.19	841	−6.66	2.55	gl (62), cpx (35.2), mag (1.8), ilm (<1)
K47	0.017	0.2	2.0	0.17	756	−6.76	2.45	–
K54	0.017	0.2	2.0	0.17	756	−6.76	2.45	gl, cpx, mag
K51	1.7	0.2	2.1	0.09	399	−7.31	1.90	gl (70), ol (<1), cpx (29.2), mag (<1)
K57	6.1	0.2	2.7	0.28	1,250	−6.32	2.89	gl (67), ol (<1), cpx (30.4), mag (1.4), ilm (<1)
K44	17.7	0.2	2.2	0.21	926	−6.58	2.63	gl (65), ol (<1), cpx (30.1), mag (1.5), ilm (2.5)
K1	24.0	0.2	2.0	0.18	809	−6.70	2.51	gl (67), ol (<1), cpx (30.3), mag (1.8), ilm (<1)
K74	24+	0.2	2.3	0.22	989	−6.52	2.69	gl (66), ol (<1), cpx (30.5), mag (1.5), ilm (<1)
K75	24+	0.2	3.0	0.32	1,425	−6.21	3.01	gl (65), cpx (32.5), mag (2.4)

[a] All experiments performed by heating up the starting glass to 1,100°C except runs marked with "24+" performed out of a superliquidus melt (two step experiments, see text)

[b] H_2O content in glass measured with the "by-difference method"

[c] Calculation of aH_2O, fH_2O, log fO_2, ΔQFM see paragraph "calculation of oxygen fugacity"

[d] Numbers in parenthesis show phase proportions calculated via mass balance, for abbreviations, see Table 2

The results show that the same crystalline phases and nearly identical phase proportions are observed in all runs with a duration of more than 100 min at $XH_2O = 0.2$ and in all runs with a duration of more than 3 h at $XH_2O = 0$ (Table 6). The crystalline phases olivine, clinopyroxene, plagioclase (at $XH_2O = 0$) and oxides are large enough for

a qualitative EMP analysis in experiments longer than 100 min. The size of crystals increases with increasing run duration but the phase assemblage and the phase compositions remain constant. The composition of olivine and clinopyroxene crystals analyzed in the experimental products with $XH_2O = 0$ and for run durations or 1.7, 3, 6 and 24 h are nearly identical (X_{Fo} is 76–78; Mg# in clinopyroxene is 80–83; eTable 4). The glass compositions are also nearly identical, but the quality of the analyses (small crystals and small glass pools) did not allow us to calculate the phase proportions by mass balance for the 1.7 h experiment.

All experiments performed in this study with compositions OB93, 35R2 and KGL2 were conducted by heating up the capsule directly to the desired temperature, except three experiments (K73, K74 and K75; Table 6) which were performed in two steps, starting from a temperature of 1,250°C (at which liquidus conditions are expected) for 24 h (first step) and following with a temperature of 1,100°C for 24 h (second step). The comparison of the experimental results from the two types of experiments may be helpful to check if serious undercooling problem may occur or if metastable phase may crystallize. The proportion and the composition of phases observed in the two experiment types (one-step or two-steps experiments) are nearly identical (Table 6). At $XH_2O = 0$ olivine is observed in very small amounts in the one-step experiment and is not observed in the two-steps experiment. At $XH_2O = 0.2$, olivine is observed in very small amounts in a one- and in two-step experiments and is not observed in another two-step experiment. Considering that olivine is observed in very low proportions, the experimental conditions must be very close to those required for the beginning of crystallization of olivine and the differences (olivine present or not) may be due to very small changes in water activity or oxygen fugacity, which cannot be avoid.

To summarize, our experiments with different duration and different approaches (one-step and two-steps) indicate that near equilibrium conditions were obtained in less than 2 h at $XH_2O = 0.2$ and less than 3 h at nominally dry conditions at 1,100°C with composition KGL2. In this study, kinetic experiments were not conducted at lower temperatures but phase relations were investigated at temperatures as low as 960°C at reducing conditions (short duration). However, the H_2O activities in the low temperature experiments were higher than those prevailing in the kinetic experiments and the duration in the low temperature reducing experiments was up to 6 h. Thus, we do not expect the crystallization of metastable phases or strong departure from equilibrium conditions in the experimental products obtained at reducing conditions.

Phase relations for the tholeiitic basalt (35R2)

All experimental conditions and run products for the crystallization experiments with the tholeiitic basalt (35R2) are summarized in Tables 2 and 3. The phases identified at oxidizing conditions (log $fO_2 \sim \Delta QFM + 4$) include clinopyroxene, plagioclase, amphibole, ilmenite and magnetite. Under reducing conditions (log $fO_2 \sim$ QFM), magnetite is absent in the experiments.

$log\ fO_2 \sim \Delta QFM + 4$

Under oxidizing conditions (Fig. 3a) magnetite is the liquidus phase for the entire range of water contents in the melt. At high water contents in the melt the crystallization sequence is: magnetite (<1,120°C), clinopyroxene (≤1,080°C) and amphibole (<1,000°C). For low water contents (<3.0 wt% H_2O) plagioclase and ilmenite crystallize after magnetite and clinopyroxene. In one experiment at 1,000°C, the amount of melt was below 1 wt% (run 111). These conditions have been assumed to be near to the solidus.

$log\ fO_2 \sim QFM$

Phase relations for reducing conditions (Fig. 3b) vary strongly from those observed under oxidizing conditions (Fig. 3a). The liquidus phase for all water contents is clinopyroxene. At $aH_2O = 1$, clinopyroxene crystallizes below 1,040°C. At low water activities ($aH_2O < 0.58$, corresponding to a H_2O concentration in the melt <6.5 wt%) clinopyroxene crystallizes at temperatures above 1,080°C. The crystallization sequence for 2.0 wt% H_2O in the melt with decreasing temperature is: clinopyroxene, plagioclase and olivine together with ilmenite (Fig. 3b). The stability field of amphibole is restricted to temperatures below 1,040°C and water contents down to 2.5 wt% H_2O.

Phase relations for the mildly alkalic basalt (OB93-190)

The run products and experimental conditions for the crystallization experiments with the mildly alkalic basalt (OB93-190) are summarized in Tables 4 and 5. The crystalline phases identified at oxidizing conditions (log $fO_2 \sim \Delta QFM + 4$) include magnetite, clinopyroxene, ilmenite, plagioclase, olivine and amphibole. Under reducing conditions (log $fO_2 \sim$ QFM), magnetite was absent in the experiments.

$log\ fO_2 \sim \Delta QFM + 4$

For water-saturated as well as for water-undersaturated conditions magnetite is the liquidus phase at log

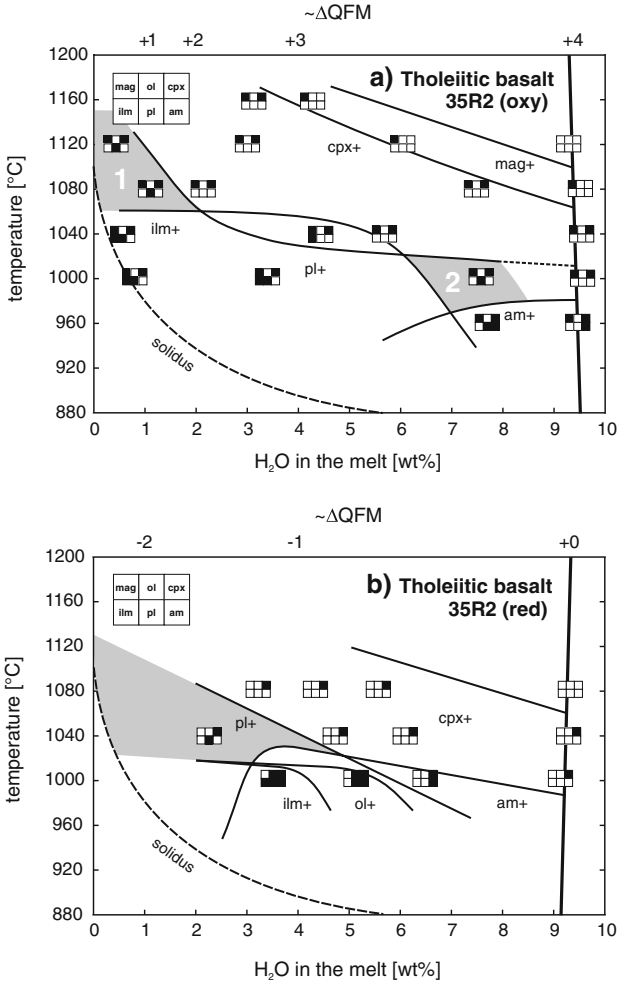

Fig. 3 Phase relations of the tholeiitic basalt (35R2) under **a** oxidizing (log $fO_2 \sim \Delta QFM + 4$ at water-saturated conditions) and **b** reducing conditions (log $fO_2 \sim$ QFM at water-saturated conditions) shown as a function of wt% H_2O in the melt versus temperature at 500 MPa. The values indicated on the *top* the diagram show approximately the evolution of fO_2 as a function of the H_2O concentration in the melt. The *heavy vertical line* represents the H_2O saturation curve. *Curves* are labeled with mineral names lying inside their stability fields. For orientation, an estimated *solidus curve* for water-undersaturated conditions is additionally plotted in the diagram. The *grey* fields represent the conditions that match the observed phase assemblages in the natural lavas used as starting materials. *mag* magnetite, *ol* olivine, *cpx* clinopyroxene, *ilm* ilmenite, *pl* plagioclase, *amph* amphibole

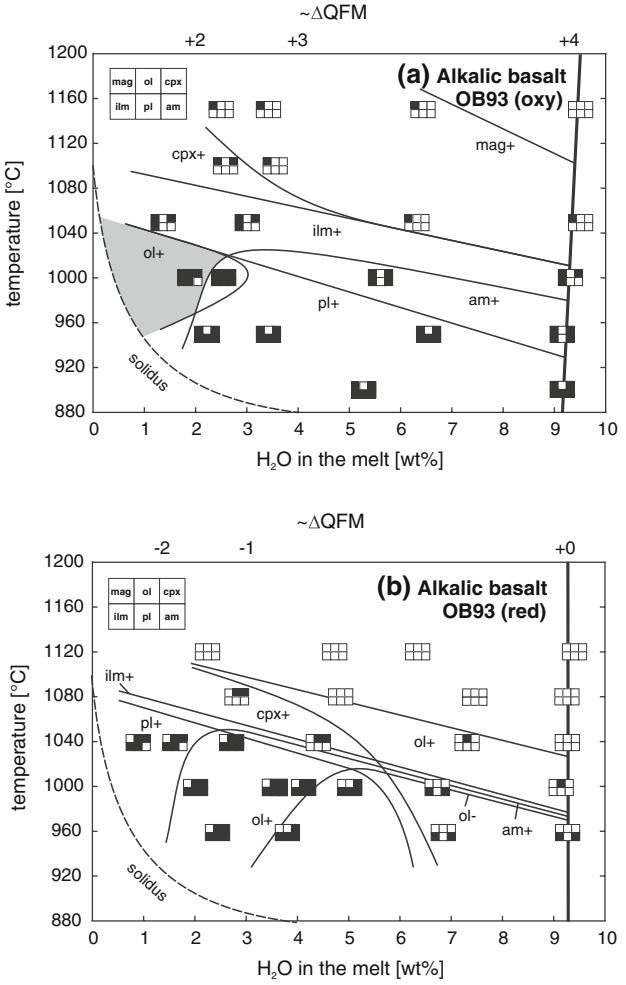

Fig. 4 Phase relations of the alkali basalt (OB93-190) under **a** oxidizing (log $fO_2 \sim \Delta QFM + 4$ at water-saturated conditions) and **b** reducing conditions (log $fO_2 \sim$ QFM at water-saturated conditions) shown as a function of wt% H_2O in the melt versus temperature at 500 MPa. Additional remarks: see Fig. 3. For abbreviations, see Fig. 3

$fO_2 \sim \Delta QFM + 4$. At water-saturated conditions magnetite crystallizes above 1,050°C; for melt H_2O contents <4 wt%, magnetite crystallizes above 1,100°C (Fig. 4a). With decreasing temperature and at high H_2O contents, clinopyroxene crystallizes together with ilmenite followed by amphibole and finally plagioclase. At lower aH_2O, clinopyroxene crystallizes before ilmenite. Amphibole is not stable above 1,040°C but melts containing water contents as low as 2.0 wt% H_2O are in equilibrium with amphibole (Fig. 4). Olivine is only stable in two experiments at 1,000°C with water contents in the melt <3 wt% (Fig. 4).

log $fO_2 \sim QFM$

In contrast to the results under oxidizing conditions olivine is the liquidus phase for all water contents at log $fO_2 \sim \Delta QFM$ (Fig. 4). At $aH_2O = 1.0$, olivine has been observed in an experiment at 1,000°C. Olivine is not stable at 1,040 and 960°C, indicating a restricted stability range between these two temperatures. At lower aH_2O (water content of the melt in the range 5.0–7.5 wt%), the stability interval of olivine is shifted to slightly higher temperatures. At strongly reduced aH_2O (water content of the melt lower than 5.0 wt%), the stability interval increases

(920°C < T < 1,120°C). Ilmenite and amphibole start to crystallize at similar temperatures at high aH_2O (Fig. 4). The stability curve of clinopyroxene depends strongly on the water content in the melt. At low temperatures (<1,000°C) clinopyroxene is only stable up to 6–7 wt% H_2O in the melt. The stability field of plagioclase does not differ strongly from that of clinopyroxene (Fig. 4). Amphibole is stable in the experiments containing H_2O contents in the melt down to 2 wt% H_2O.

Phase compositions

Clinopyroxene

For both basalts (tholeiitic 35R2 and alkalic OB93-190) clinopyroxene is one of the most abundant minerals in the experiments. The synthesized pyroxenes are Al-rich augites (after Morimoto et al. 1988; see eTables 2, 3). In all experiments a strong influence of fO_2 on the pyroxene composition is observed (Fig. 5). The synthesized augites under oxidizing conditions (log fO_2 ~ ΔQFM + 4) contain less Fe and more Mg than under reducing fO_2 (log fO_2 ~ QFM). There is also a positive temperature dependence of the Mg# of the clinopyroxenes for both redox conditions and different XH_2O, which is in good agreement with previous studies of Toplis and Carroll (1995) and Berndt et al. (2005). Furthermore, the experiments show an influence of the aH_2O on the CaO content of the pyroxenes (see eTable 4). For the tholeiitic basalt (35R2), the CaO content of the pyroxenes increases at a constant temperature of 1,000°C under oxidizing conditions from 20.6 wt% (XH_2O_{in} = 0.4) to 22.9 wt% (XH_2O_{in} = 1.0). Under reducing conditions this effect is stronger (at 1,000°C from 17.5 wt% CaO up to 22.1 wt%; eTable 3b). These observations are in good agreement with other previous experimental studies (e.g., Gaetani et al. 1993; Freise et al. 2003).

Plagioclase

For both redox conditions (log fO_2 ~ ΔQFM + 4 and log fO_2 ~ QFM) and compositions (OB93-190 and 35R2), the An content increases with increasing aH_2O and temperature (see eTables 2 and 3), as demonstrated in previous studies (e.g., Carmichael et al. 1974; Sisson and Grove 1993). In the experiments with the mildly alkalic basalt (OB93-190) an indirect influence of the oxygen fugacity on the composition of the plagioclases is observed. As shown in Fig. 6, it appears that An-rich plagioclase only crystallizes under oxidizing conditions. This can be explained by the changing of the stability field of plagioclase. With increasing fO_2, the plagioclase stability field expands toward higher water contents in the melt. The An content is known to increase with aH_2O (see above). Thus, the conditions necessary to form the most An-rich plagioclases are attained at high fO_2 and high water contents in the melt (Figs. 3, 4).

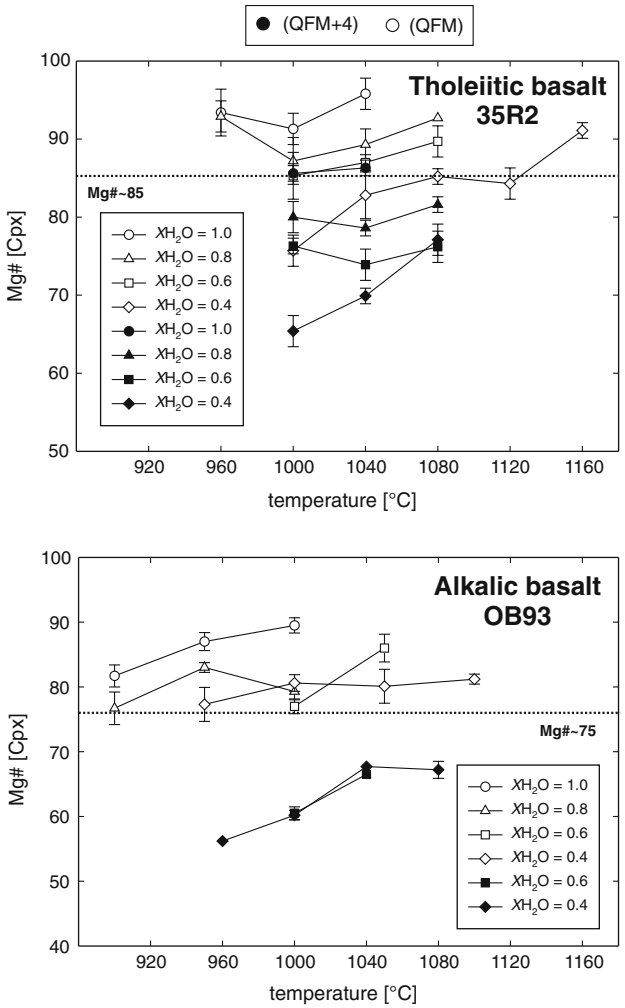

Fig. 5 Mg# of experimental clinopyroxene of **a** 35R2 and **b** OB93-190 as a function of temperature, XH_2O and fO_2. *Error bars* correspond to the standard deviation of average clinopyroxene compositions from multiple microprobe measurements. *Dashed line* represents the average Mg# of the natural phenocrysts

Olivine

Systematic variation of olivine compositions can be documented only for OB93-190, because olivine is observed in only one single experiment (run 131) with 35R2. As expected from other studies, the Fo content (X_{Fo}) of the synthesized olivine decreases with decreasing temperature (e.g., from Fo_{74} at 1,080°C down to Fo_{54} at 1,000°C, runs 91 and 87 with 2.9 and 4.1 wt% H_2O in the melt, respectively, eTable 2b). In our experiments, decreasing water content is coupled to decreasing fO_2. Consistently, the Fo

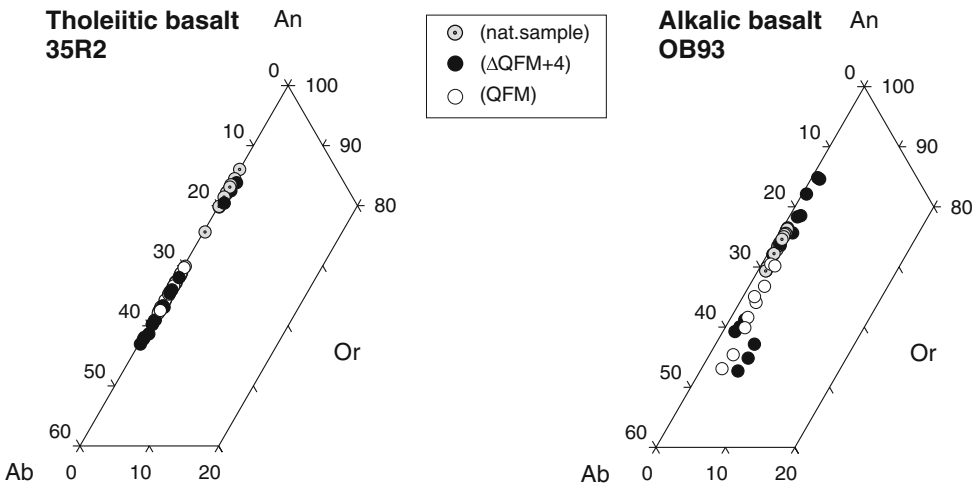

Fig. 6 Experimental plagioclase composition of **a** 35R2 and **b** OB93-190 at different oxygen fugacities plotted in a feldspar ternary diagram (An–Ab–Or)

content decreases with decreasing water content in the melt (at 1,040°C from Fo_{74} at ~7.0 wt% H_2O to Fo_{60} at ~0.9 wt% H_2O; runs #81 and #104, respectively, Table 4) and decreases with decreasing fO_2 (at 1,000°C in runs with similar water content in the melt from Fo_{88} at ΔQFM + 4 to Fo_{54} at QFM).

Amphibole

Following the classification of Leake et al. (1997), all our synthesized amphiboles are Ti-rich kaersutites (see eTables 2 and 3). The TiO_2 contents of the kaersutites vary little as a function of temperature in the experiments with both basalts (35R2 and OB93-190) at a given aH_2O and fO_2 (e.g., $XH_2O_{in} = 1.0$ and log $fO_2 \sim$ ΔQFM + 4 from TiO_2 = 2.02 wt% at 900°C up to 2.15 wt% at 950°C). The most important changes in kaersutite composition result from changing the fO_2. Decreasing the fO_2 from ΔQFM + 4 down to QFM at a constant temperature of 960°C and water-saturated conditions leads to increasing TiO_2 contents in the kaersutites (from 2.15 wt% up to 3.47 wt%) in alkalic basalt. Furthermore, amphiboles synthesized under oxidizing conditions have the highest Mg# (Fig. 7).

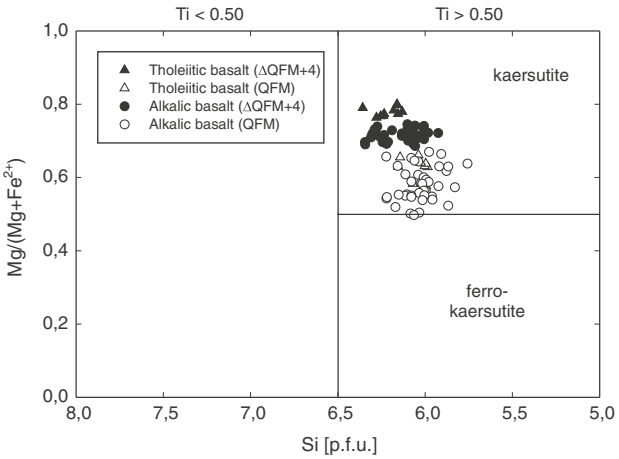

Fig. 7 Experimental amphibole composition of 35R2 and OB93-190 at different oxygen fugacities after the nomenclature of Leake et al. (1997)

Glass

The concentrations of SiO_2, TiO_2, FeO* and $Na_2O + K_2O$ in the experimental glasses are plotted against temperature in Fig. 8. For both samples the same qualitative trends are observed in the residual melt compositions.

The SiO_2 contents in the residual melts increase with decreasing temperature (Fig. 8). Furthermore, the SiO_2 content increases at a constant temperature with decreasing aH_2O. Figure 8 also shows a strong influence of the fO_2 on the SiO_2 contents of the residual melts. Under oxidizing conditions (log $fO_2 \sim$ ΔQFM + 4) the melts of both basalts have a higher SiO_2 content than observed under reducing conditions (log $fO_2 \sim$ QFM). This SiO_2-enrichment in melts could be related to a change of crystal content in the experimental products at reducing and oxidizing conditions (e.g., Scaillet and McDonald 2003) and also to different modes of the crystal population (especially proportions of amphibole, clinopyroxene and plagioclase).

The TiO_2 contents of the melts depend strongly on the crystallization of ilmenite and kaersutite (Fig. 8). At high temperatures, the TiO_2 contents in the melts are nearly identical for all experiments. With decreasing temperature a general trend of decreasing TiO_2 contents is observed for both redox conditions and is related to the crystallization of ilmenite and kaersutite. At reducing conditions the TiO_2 contents in the glasses are higher because of the fractionation of Ti-poor kaersutites and ilmenites. Additionally, the

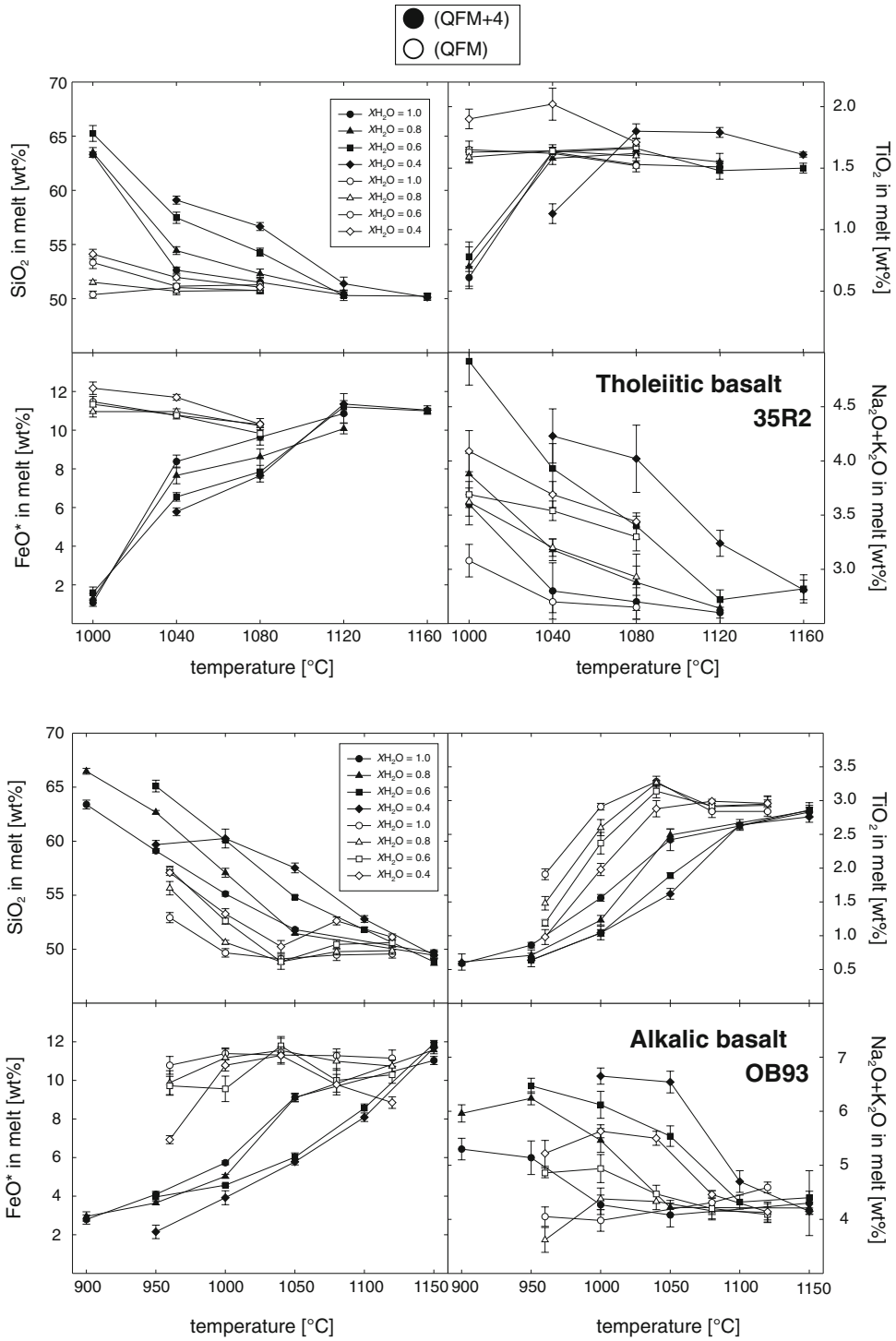

Fig. 8 Experimental glass compositions of **a** 35R2 and **b** OB93-190 as a function of temperature at different XH_2O and fO_2. *Error bars* correspond to the standard deviation of average glass compositions from multiple microprobe measurements. Note that all analyses are normalized to 100 wt%

TiO_2 contents increase with decreasing aH_2O at constant temperature which may be an indirect effect of fO_2 (fO_2 decreases with decreasing aH_2O).

Figure 8 reports a strong influence of fO_2 on the FeO* contents in the residual melts for both samples (OB93-190 and 35R2). Under reducing conditions the FeO* content in the melts is nearly constant and increases slightly for 35R2 with decreasing temperature. This trend is explained by the absence of magnetite in the crystallizing assemblage. In contrast, the FeO* content decreases strongly with decreasing temperature under oxidizing conditions (Fig. 8). This trend is mainly controlled by the crystallization of magnetite. A similar trend of FeO* enrichment in the melts is observed in Berndt et al. (2005).

The evolution of total alkali contents ($Na_2O + K_2O$) of the glasses shows a general increase with decreasing

temperature (Fig. 8). The evolution of total alkali content in the melts is mainly dependent on the crystal content (or portion) since no mineral phase incorporates these elements in significant amounts (except for Na in plagioclase). Little change in $Na_2O + K_2O$ content is observed for $XH_2O = 1.0$ because of the low crystal content in these experiments. For both oxygen fugacities, an influence of XH_2O on the total alkali content of the melts is observed. At a constant temperature of 950°C and oxidizing conditions $Na_2O + K_2O$ decreases with decreasing XH_2O from 5.1 wt% ($XH_2O = 1.0$) down to 0.6 wt% ($XH_2O = 0.6$). Additionally, the melts obtained under oxidizing conditions have higher $Na_2O + K_2O$ than those obtained under reducing conditions at the same temperature (difference of ~1.0 wt% at 1,000°C and $XH_2O = 0.4$). As shown for the SiO_2 content this difference is not a direct result of increasing amount of crystals but must also result from the different proportions of solid phases in the experiments (especially plagioclase).

Discussion

Experiments versus MELTS

MELTS (Ghiorso and Sack 1995; Ghiorso 1997) has been used to calculate the equilibrium crystallization diagram of the alkali basalt (OB93-190) at 500 MPa and oxidizing conditions ($\log fO_2 \sim \Delta QFM + 4$) over the studied range of temperatures and water contents in the melt to compare the predictions with the experimental results (Fig. 9). MELTS correctly predicts magnetite as the liquidus phase. However, the calculated crystallization temperature of clinopyroxene is ~60 to 80°C higher than that observed in the experiments. The plagioclase stability field fits correctly the experiments at low aH_2O but fails at high aH_2O. Ilmenite, an important oxide phase, and kaersutite are stable in the experiments, but are never predicted by MELTS. MELTS predicts orthopyroxene (not observed in the experiments) instead of olivine, which is synthesized in the experiments. Discrepancies are also apparent between the experimental and calculated H_2O solubility (see nearly vertical curve on Fig. 9). The general discrepancies between experimentally determined and calculated phase stability fields are due to the lack of data on hydrous basalt at low pressure in the database used for MELTS.

Effect of fO_2 on phase relations

Changing fO_2 in the experiments with natural basalts from the Kerguelen Plateau and Archipelago causes drastic changes in phase chemistry and in phase relations as previously described. To illustrate these variations, selected

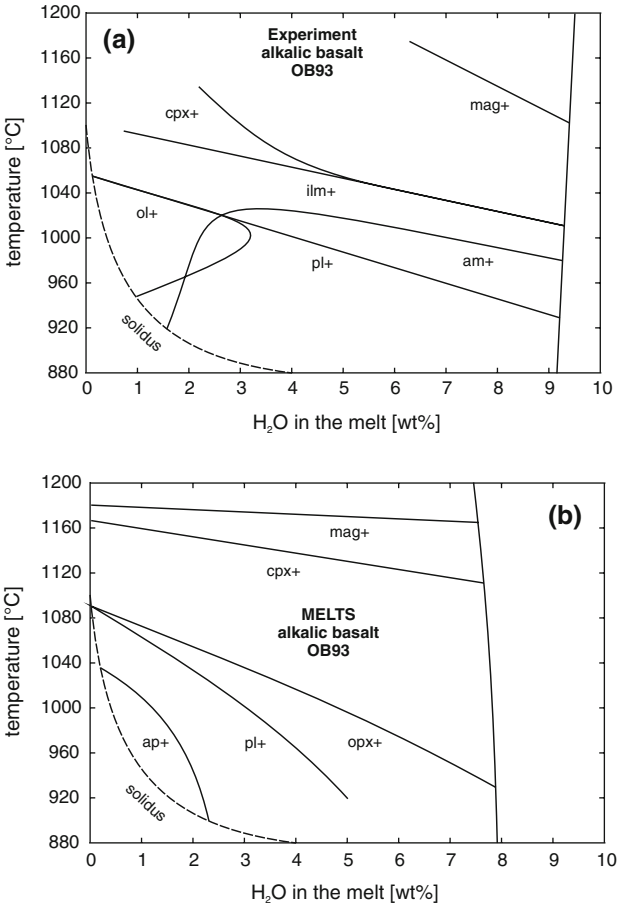

Fig. 9 **a** Experimental phase relations of alkali basalt (OB93-190) at 500 MPa and oxidizing conditions ($\log fO_2 \sim \Delta QFM + 4$). **b** Predicted phase diagram of OB93-190 using MELTS (Ghiorso and Sack 1995)

stability curves of minerals are plotted in Fig. 10. For the more alkali-rich composition OB93-190, the stability field of clinopyroxene increases with increasing fO_2. The change of the stability field is particularly marked at high water activities. Considering the experimental conditions, the differences in the crystallization temperature of clinopyroxene in the tholeiitic basalt (35R2) at $\log fO_2 \sim$ QFM and $\log fO_2 \sim \Delta QFM + 4$ may be interpreted with caution (there are little data to bracket the crystallization curve of clinopyroxene at reducing conditions).

As expected, the olivine stability field increases with decreasing fO_2 from $\Delta QFM + 4$ down to QFM (Fig. 10), which is explained by the preferential incorporation of Fe^{2+} in olivine and by the high Fe^{2+}/Fe^{3+} ratio in the melts under reducing conditions. It is interesting to note that olivine is not observed in the less differentiated composition (35R2) under oxidizing conditions, whereas it has a restricted stability field for the more differentiated sample (OB93-190). This differs from the classical view in which the olivine stability field decreases with increasing

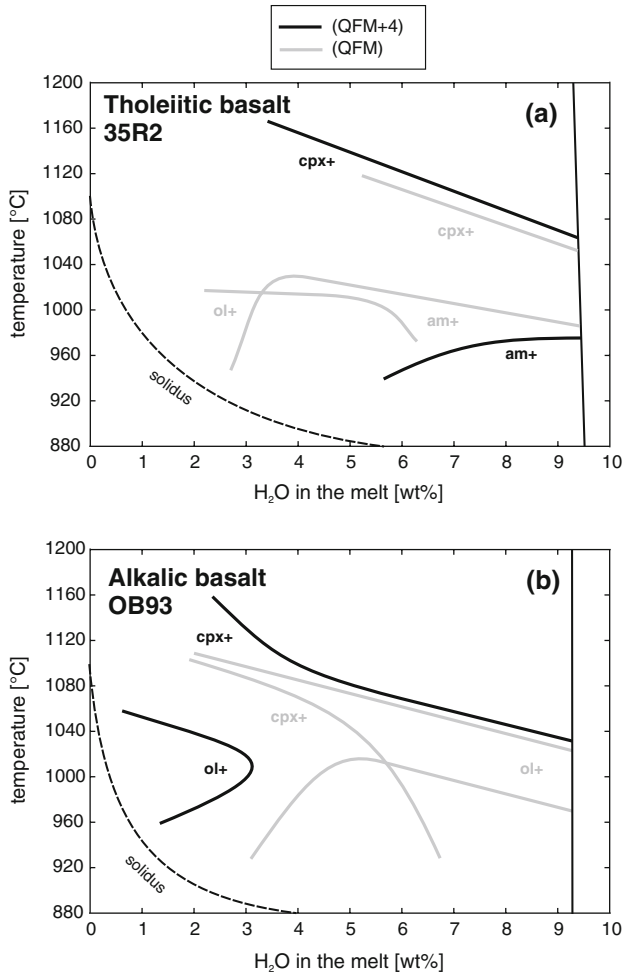

Fig. 10 Comparison of phase relations from **a** tholeiitic basalt (35R2) and **b** alkalic basalt (OB93-190) at 500 MPa under different fO_2. *Black lines* represents log $fO_2 \sim \Delta$QFM + 4 and *grey lines* log$fO_2 \sim$ QFM. Only selected stability curves are shown in the figure. The amphibole stability fields in the alkalic basalt were found to be similar at reducing and oxidizing conditions and are not reported in Fig. 10b

differentiation (e.g., Toplis and Carroll 1996; Caroff et al. 1997; Grove et al. 2003) and may be due to the relatively low SiO_2 content of OB93-190. The importance of this observation for the differentiation trend of alkali-rich basalts is discussed below.

Phase relations for the mildly alkalic basalt OB93-190 show that within error the stability field of amphibole does not change with decreasing oxygen fugacity from log $fO_2 \sim \Delta$QFM + 4 to log $fO_2 \sim$ QFM (Fig. 4). For the tholeiitic basalt 35R2, the comparison of the kaersutite stability field is difficult because of the lack of experiments at low temperatures (Figs. 3, 10). The stability field of amphibole is well constrained for three phase diagrams (Figs. 3, 4). For both starting compositions it is worth noting that the upper crystallization temperature of amphibole first increases with decreasing water content in the melt down to approximately 2–3 wt% H_2O in the melt. Amphibole is clearly stable in OB93-190 at water contents as low as 2 wt% H_2O. This differs from the amphibole stability field in basaltic and calc-alkaline systems (e.g., Holloway and Burnham 1972; Dall'Agnol et al. 1999; Costa et al. 2004; Berndt et al. 2005). This difference may be explained by the different whole rock composition, which is relatively TiO_2-rich when compared to the other compositions, thus leading to the crystallization of kaersutite instead of pargasite. The increased stability field of amphibole with decreasing fO_2 may also be related to the higher TiO_2 content of amphiboles synthesized at low fO_2.

Effect of fO_2 on differentiation trends

Figure 11 shows the FeO*/MgO weight ratio versus SiO_2 content of the residual melts at the different oxygen fugacities examined in this study. The glasses obtained under reducing conditions (QFM) show a strong increase in melt FeO*/MgO ratio with increasing SiO_2 content. These melts follow a tholeiitic differentiation trend after the classification of Miyashiro (1974) due to the absence of magnetite crystallization. The residual melt compositions of the experiments performed under oxidizing conditions coexist widely with magnetite and are consequently depleted in FeO* following a calc-alkaline differentiation trend. The influence of the whole rock compositions on the differentiation path can be shown by comparing the trend of the residual melts for both basalts (35R2 and OB93-190). At low fO_2, the SiO_2 content of the residual melts in 35R2 remains below 55 wt% SiO_2 and is slightly higher for some experiments in OB93-190 (up to 58 wt% SiO_2). At oxidizing conditions the FeO*/MgO ratio is higher in the residual melts of 35R2 than in those of OB93-190 (Fig. 11).

Fe/Mg partitioning between clinopyroxene and melt

The clinopyroxene/melt partitioning of Fe–Mg, expressed as $K_{DFe-Mg}^{Cpx\text{-}melt}$ (defined as $X_{Cpx\text{-}FeO}/X_{melt\text{-}FeO} \times X_{melt\text{-}MgO}/X_{Cpx\text{-}MgO}$) is commonly used to estimate the equilibrium compositions of these phases in basaltic systems. For example for the Mont Crozier section of the Kerguelen Archipelago, Damasceno et al. (2002) assumed a $K_{DFe-Mg}^{Cpx\text{-}melt}$ of 0.23 ± 0.05 to estimate equilibrium compositions of the clinopyroxene phenocrysts, following the results of Grove and Bryan (1983) and Toplis and Carroll (1995) obtained for basaltic compositions. However, Hoover and Irvine (1977) noted a slight compositional effect on the partition coefficient of iron and magnesium between basaltic liquids and pyroxenes. This is confirmed in this study. Figure 12 shows the $Mg\#_{melt}$–$Mg\#_{clinopyroxene}$ relations for the experimental run products for both compositions (35R2

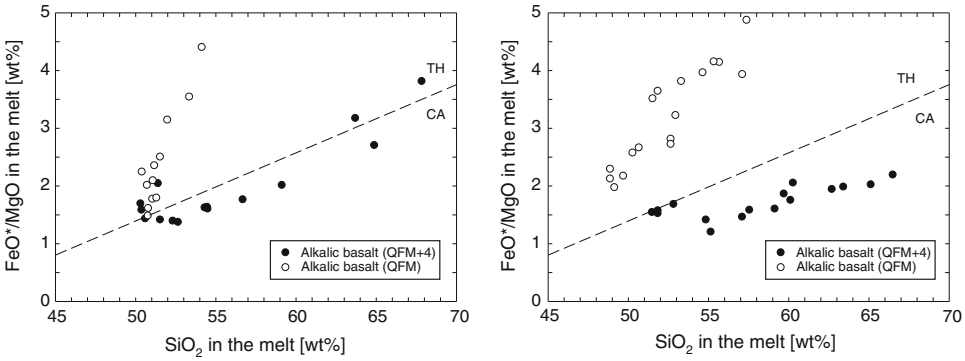

Fig. 11 FeO*/MgO weight ratios versus SiO_2 content of the residual melts obtained at different oxygen fugacities. The glasses obtained under reducing conditions (QFM) show a strong increase in melt FeO*/MgO ratio with increasing SiO_2 content. *Dashed line* delimitates the calcalkaline (*CA*) from the tholeiitic (*TH*) field

and OB93-190). The Mg# of the melt has been calculated taking into account the ferric iron content of the liquid as estimated using Kress and Carmichael (1991). The ferric iron content of clinopyroxene has been estimated from the stoichiometry of pyroxenes. For both samples 35R2 and OB93-190 a general trend of decreasing $Mg\#_{clinopyroxene}$ with decreasing $Mg\#_{melt}$ is observed (Fig. 12). The K_D value for the clinopyroxenes of the tholeiitic basalt (35R2) is 0.22 ± 0.05. This value does not change significantly with the water content of the melt and the compositional pairs plot within the predicted field (K_D of 0.23 ± 0.05) of the partition coefficient determined by Toplis and Carroll (1995). In contrast, the Fe/Mg ratios of the clinopyroxenes from the alkali basalt (OB93-190) are systematically lower (K_D of 0.41 ± 0.07). The identical K_D values for the tholeiitic basalt (35R2) and basalt SC1 from Toplis and Carroll (1995) can be explained by similar bulk compositions. The shift to higher K_D values for the alkali basalt (OB93-190) must be influenced by the different whole rock composition because the experimental parameters for both basalts were identically. A similar trend was observed by Toplis (2005) for olivine partition coefficients with lower K_D values for alkali-rich compositions.

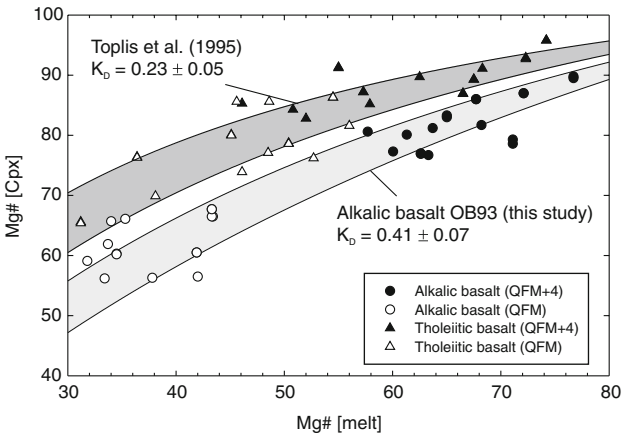

Fig. 12 Mineral-melt Fe/Mg equilibrium diagram for the experimental clinopyroxenes of 35R2 and OB93-190 under different oxygen fugacities. The equilibrium field for Fe/Mg exchange between clinopyroxene and basaltic melt (0.23 ± 0.05; Toplis and Carroll 1995) is shown as the heavy shaded field. Additionally, the equilibrium field for Fe/Mg exchange between clinopyroxene and the melt of OB93-190 is shown as the light shaded field. The calculation of Fe^{2+} in the melts was performed after Kress and Carmichael (1991). Fe^{2+} in the clinopyroxenes was determined stoichiometrically

Pre-eruptive conditions

Tholeiitic basalt 35R2

The natural phenocryst assemblage for the tholeiitic basalt, plagioclase and clinopyroxene, can be reproduced under both oxidizing and reducing conditions (Fig. 3). Considering that water contents in basalts generated from the mantle are expected to be low (e.g., Danyushevsky et al. 2002; Wallace 2002), temperatures above 1,060–1020°C (see grey fields) are required in the magma chamber of tholeiitic basalt (35R2) to reproduce the natural phase assemblage, assuming that the storage conditions are close to 500 MPa. At oxidizing conditions magnetite may have been stable together with clinopyroxene and plagioclase. Magnetite is observed in the natural sample but it is difficult to discriminate if this phase belongs to the phenocryst assemblage or to the groundmass.

The pre-eruptive water content for the tholeiitic magmas can also be estimated from the comparison of the An contents of the experimental and natural plagioclases (e.g., Helz 1973; Martel et al. 1998; Klimm et al. 2003). The natural plagioclase phenocrysts of sample 35R2 show a systematic zonation with average core composition of An_{83} (variation between An_{81} and An_{86}) and a less calcic rim ($An_{65–69}$). The An contents of the experimental plagioclases ($An_{61–67}$) obtained in the temperature range 1,040°C up to 1,120°C and with melt water contents of 0.5 and 1.2 wt% H_2O (log fO_2 ~ ΔQFM and ΔQFM + 1.5) and 2.3 wt% (log fO_2 ~ ΔQFM − 1.6) are nearly identical to the composition of natural plagioclase rims ($An_{65–69}$). Thus, the composition of plagioclases in experiments with plagioclase and clinopyroxene, as crystalline phases only, is in

agreement with the natural phenocryst composition. It is difficult to constrain the melt water content from the experimental data set. However, in the temperature range of 1,040°C up to 1,120°C, plagioclases with $An_{65–69}$ could not crystallize from melts with water contents higher than 5 wt% H_2O. In our experimental products, the high An contents of the natural plagioclase cores could only be reproduced under high water contents in the melt. Because of these unrealistic high water contents, the plagioclase cores may have crystallized from a melt with a composition which is different from the investigated bulk composition and may be inherited.

The prevailing fO_2 during the crystallization of clinopyroxenes from 35R2 can be estimated by comparing the Mg# of the synthetic clinopyroxenes with the natural phenocrysts (Fig. 5). At reducing fO_2, the Mg# of the clinopyroxenes was reproduced only in one run at water-saturated conditions (run 132; Table 3), which is not realistic. Under oxidizing conditions, the natural Mg# was reproduced only in runs at low XH_2O ($\leq$0.6). The temperatures and calculated fO_2 of the runs with low water activities ($XH_2O = 0.4$) is log $fO_2 \sim \Delta QFM + 0.4$, 1,040°C (run 115); log $fO_2 \sim \Delta QFM + 1.5$, 1,080°C (run 119) and log $fO_2 \sim \Delta QFM + 0.1$, 1,120°C (run 123). The melt water contents of these experiments are realistic (0.5 and 1.2 wt% H_2O) suggesting that the conditions prevailing during crystallization of clinopyroxenes were moderately oxidizing (log $fO_2 \sim \Delta QFM$ up to $\sim \Delta QFM + 1.5$). It is emphasized that the Mg# of the natural clinopyroxenes can only be reproduced at more reducing conditions if the melt H_2O content is unrealistically high.

Alkali basalt OB93-190

The natural phenocryst assemblage of the mildly alkalic basalt consists mainly of plagioclase, and minor amounts of olivine, clinopyroxene, ilmenite and magnetite. Petrographic observations show that clinopyroxene is usually not idiomorphic (rounded shape). Thus, it is not clear whether or not this mineral belongs to the equilibrium phase assemblage.

The presence of oxides in the phenocryst assemblage indicates that oxidizing conditions were prevailing since ilmenite coexisting with magnetite has only been observed at log fO_2 above $\sim\Delta QFM + 1$ (Fig. 4). Assuming that clinopyroxene is an equilibrium phase, the natural phenocryst assemblage can only be reproduced at oxidizing conditions (Fig. 4). An estimation of the prevailing fO_2 during the crystallization of clinopyroxenes in composition OB93-190 can also be made directly by comparing the Mg# of the natural and experimental clinopyroxenes (Fig. 5). Figure 5 shows that the natural Mg# of the clinopyroxene phenocrysts is never reproduced at reducing conditions. However, the composition of clinopyroxenes synthesized under oxidizing conditions is close to that of the natural minerals especially for experiments 53, 59 and 61 (eTable 2). The temperatures and calculated fO_2 of these runs is log $fO_2 \sim \Delta QFM + 2.6$, 1,000°C (run 53); log $fO_2 \sim \Delta QFM + 2.0$, 950°C (run 59) and log $fO_2 \sim \Delta QFM + 3.6$, 900°C (run 61). The phase relation assemblage constrains the pre-eruptive temperature between 950 and 1,050°C. Thus, an oxygen fugacity of log $fO_2 \sim \Delta QFM + 2.0$ up to 2.6 can be estimated for the low pressure magma chamber of the alkali basalt (OB93-190) if melt water contents are as high as 2.2 and 2.5 wt% H_2O, respectively. Assuming lower H_2O contents as indicated by Wallace (2002), the fO_2 extrapolated from our experimental data set suggests that oxygen fugacities near log $fO_2 \sim \Delta QFM + 1$ up to $\sim\Delta QFM + 2$ may prevail for the crystallization of the mineral assemblage of the alkalic basalt (OB93-190). Figure 5 confirms that the natural clinopyroxene composition from the alkalic basalt (OB93-190) could be in equilibrium with the bulk melt composition at a log fO_2 above $\sim\Delta QFM + 2$. The An content of the plagioclases synthesized at oxidizing conditions and low H_2O activities (An_{77} at 1,000°C, run 53; see eTable 2a) are consistent with the natural compositions of the plagioclase rims ($An_{69–76}$) and confirm that H_2O contents in the melt are lower than 2.5 wt% (plagioclase cores are only slightly more calcic, up to An_{79}). Geochemical or petrological studies constraining the H_2O contents of the alkalic Mont Crozier magmas (e.g., OB93-190) are not available. However, Wallace (2002) determined $\sim$0.7 wt% H_2O for the most alkali-rich compositions in basaltic glasses from the Site 1140, ODP Leg 183.

Assuming that clinopyroxene does not belong to the equilibrium phase assemblage, the oxygen fugacity should be extremely low. As shown above, the stability field of clinopyroxene decreases with decreasing fO_2 (Fig. 10). Concomitantly, the stability field of plagioclase increases slightly with decreasing fO_2. Thus, a stability field in which plagioclase is coexisting with olivine could theoretically be obtained at extremely low oxygen fugacities and low water activities. In this hypothesis, the composition of the natural clinopyroxene phenocrysts would be out of equilibrium with the coexisting melt (Fig. 4). An additional possibility to check for the oxygen fugacity prevailing in OB93-190 would be to consider the olivine compositions. However, no satisfying analysis of olivine phenocrysts for OB93-190 could be obtained (strong alteration).

General observations

The comparison of the natural rocks and experimental products in this study indicates that relatively high fO_2 conditions may prevail during the differentiation of basalts

of the Kerguelen Archipelago and Plateau. A relatively high fO_2 condition for the Kerguelen magmas ($\sim$1 to 2 log units above the QFM buffer) is in good agreement with other studies on OIB and LIP basalts. The fO_2 measurements of Ballhaus (1993) are based on olivine–orthopyroxene–spinel oxygen sensors and show a fO_2 interval between QFM and ΔQFM + 2 for OIB. In addition, Ryabchikov et al. (2001) also found relatively oxidized fO_2 conditions of $\sim\Delta$QFM + 1.5 for plateau basalts of the Siberian Igneous Province based on spinel compositions. Some possible explanations for such oxidized melts are (1) early degassing of volatiles (e.g., CH_4, H_2, CO) which leads to a relative oxidation of the melts and (2) differentiation of primitive melts out of the graphite stability field along fO_2-decompression paths controlled by continuous Fe^{3+}–Fe^{2+} solid-melt equilibria. These equilibria will involve an increase in fO_2 relative to the graphite saturation surface and relative to the QFM buffer (Ballhaus 1993).

Role of clinopyroxene in the differentiation of Kerguelen basalts

The petrologic evolution of the mildly alkalic basaltic magmas of the Mont Crozier section on the Kerguelen Archipelago has been discussed in detail by Damasceno et al. (2002). They proposed that high-pressure, high-Al clinopyroxene crystallization played a major role during differentiation of the relatively young 24–25 Ma mildly alkalic basalts relative to the older 26–29 Ma tholeiitic-transitional basalts on the archipelago (see also Scoates et al. 2006). The thickening of both the Northern Kerguelen Plateau by continued magmatic activity from 40 to 24 Ma and by cooling of the lithosphere during movement of the plateau from a ridge-centered position to an intraplate position lead to fractionation at higher pressures (Damasceno et al. 2002).

Sample OB93-190 is a mildly alkalic basalt and the experimental phase relationships shows that early clinopyroxene fractionation can occur at 500 MPa providing that the fO_2 conditions are relatively oxidizing. The crystallization pressure for En-rich clinopyroxenes was estimated by Damasceno et al. (2002) to be above 500 MPa using the thermobarometer from Putirka et al. (1996). High pressure favors the crystallization of augite (Naumann and Geist 1999) resulting in a depletion in silica and alkali enrichment of the residual liquid. Applying the model of Putirka et al. (1996) to the experimental results shows that the pressure and temperature tend to be overestimated. The difference between the experimental and calculated pressures and temperatures is higher than the error of $\pm$30°C and $\pm$140 MPa given by Putirka et al. (1996). Thus, the crystallization pressures at which early clinopyroxene fractionation occurs may be lower than previously estimated.

Conclusions

The experiments performed in this study show a significant influence of the oxygen fugacity on the phase relations, phase chemistry and differentiation trends of two basalts (tholeiitic and mildly alkalic) from the Kerguelen LIP. On the basis of equilibrium crystallization experiments for both basalts (35R2 and OB93-190) moderately to strongly oxidizing conditions (log $fO_2 \sim \Delta$QFM + 1 to log $fO_2 \sim \Delta$QFM + 2) could be determined. Our results indicate that the crystallization of phenocrysts in the most differentiated composition (OB93-190) occurred at higher fO_2 than in tholeiitic basalt (35R2). The crystallization of clinopyroxene is enhanced under oxidizing conditions (log $fO_2 >$ QFM) and calc-alkaline differentiation trends occur only at oxidizing conditions (Figs. 10, 11). Thus, oxygen fugacity plays an important role during the differentiation of basalts in LIPs. The fO_2 plays also an important role in the generation of alkali-rich residual melts. Under oxidizing conditions (log $fO_2 >$ QFM) the enrichment of total alkalis ($Na_2O + K_2O$) as a result of differentiation is higher than at reducing fO_2.

Acknowledgments This research was carried out in the framework of the ODP "Schwerpunktprogramm" supported by the German Science Foundation (DFG, Ho1337). The ODP is sponsored by the US National Science Foundation (NSF) and participating countries under management of Joint Oceanographic Institutions (JOI), Inc. Sample 35R2 was collected during ODP Leg 183 and sample OB93-190 was collected on the Kerguelen Archipelago by D. Weis and D. Damasceno. We thank Dominique Weis for help in selecting the appropriate samples for the experimental study. We thank O. Diedrich for preparing the samples and W. Hurkuck and B. Aichinger for technical assistance.

References

Ablay GJ, Carroll MR, Palmer MR, Marti J, Sparks RSJ (1998) Basanite–phonolite lineages of the Teide Pico Viejo volcanic complex, Tenerife, Canary Islands. J Petrol 39:905–936

Albarède F (1995) Introduction to geochemical modeling. Cambridge University Press, Cambridge, p 543

Ariskin AA (1999) Phase equlilibria modeling in igneous petrology: use of COMAGMAT model for simulating fractionation of ferro-basaltic magmas and the genesis of high-alumina basalt. J Volcanol Geotherm Res 90:115–162

Ballhaus C (1993) Redox states of lithospheric and asthenospheric upper mantle. Contrib Mineral Petrol 114:331–348

Berndt J (2002) Differentiation of MOR Basalt at 200 MPa: experimental techniques and influence of H_2O and fO_2 on phase relations and liquid line of descent, Thesis. Universität Hannover

Berndt J, Liebske C, Holtz F, Freise M, Nowak M, Ziegenbein D, Hurkuck W, Koepke J (2002) A combined rapid-quench and Shaw membrane setup for internally heated pressure vessels: description and application for water solubility in basaltic melts. Am Mineral 87:1717–1726

Berndt J, Koepke J, Holtz F (2005) An experimental investigation of the influence of water and oxygen fugacity on differentiation of MORB at 200 MPa. J Petrol 46:135–167

Bohlen SR, Boettcher AL, Wall VJ (1982) The system albite–H_2O–CO_2—a model for melting and activities of water at high-pressures. Am Mineral 67:451–462

Borisova AY, Nikogosian IK, Scoates JS, Weis D, Damasceno D, Shimizu N, Touret JLR (2002) Melt, fluid and crystal inclusions in olivine phenocrysts from Kerguelen plume-derived picritic basalts: evidence for interaction with the Kerguelen Plateau lithosphere. Chem Geol 183:195–220

Botcharnikov RE, Behrens H, Holtz F (2006) Solubility and speciation of C-O-H fluids in andesitic melt at $T = 1{,}100$–$1{,}300$°C and $P = 200$ and 500 MPa. Chem Geol 229:125–143

Burnham WC (1979) The importance of volatile constituents. In: Yoder HS Jr (ed) The evolution of the igneous rocks. Princeton University Press, Princeton, pp 439–482

Carmichael SE, Turner FJ, Verhoogen J (1974) Igneous Petrology. McGraw-Hill, New York, p 739

Caroff M, Ambrics C, Maury RC, Cotten J (1997) From alkali basalt to phonolite in hand-size samples: vapor-differentiation effects in the Bouzentès lava flow. J Volcanol Geotherm Res 79:47–61

Coffin MF, Pringle MS, Duncan RA, Gladczenko TP, Storey M, Müller RD, Gahagan LA (2002) Kerguelen hotspot magma output since 130 Ma. J Petrol 43:1121–1139

Costa F, Scaillet B, Pichavant M (2004) Petrological and experimental constraints on the pre-eruption conditions of holocene dacite from Volcán San Pedro (36°S, Chilean Andes) and the importance of sulphur in silicic subduction-related magmas. J Petrol 45:855–881

Courtillot V (1999) Evolutionary catastrophes: the science of mass extinction. Cambridge University Press, Cambridge, p 173

Dall′Agnol R, Scaillet B, Pichavant M (1999) An experimental study of a lower Proterozoic A-type granite from the eastern Amazonian craton, Brasil. J Petrol 40:1673–1698

Damasceno D, Scoates JS, Weis D, Frey FA, Giret A (2002) Mineral chemistry of mildly alkalic basalts from the 25 Ma Mont Crozier section, Kerguelen Archipelago: constraints on phenocryst crystallization environments. J Petrol 43:1389–1413

Danyushevsky LV, Sobolev AV (1996) Ferric-ferrous ratio and oxygen fugacity calculations for primitive mantle-derived melts: calibration of an empirical technique. Mineral Petrol 57:229–241

Danyushevsky LV, McNeill AW, Sobolev AV (2002) Experimental and petrological studies of melt inclusions in phenocrysts from mantle-derived magmas: an overview of techniques, advantages and complications. Chem Geol 183:5–24

Devine JD, Gardener JE, Brack HP, Layne GD, Rutherford MJ (1995) Comparison of microanalytical methods for estimating H_2O contents of silicic volcanic glasses. Am Mineral 80:319–328

Dixon-Spulber S, Rutherford MJ (1983) The origin of rhyolite and plagiogranite in oceanic crust: an experimental study. J Petrol 24:1–25

Dixon JE, Clague DA, Stolper EM (1991) Degassing history of water, sulfur, and carbon in submarine Lavas from Kilauea volcano, Hawaii. J Geol 99:371–394

Dixon JE, Leist L, Langmuir CH, Schilling J-G (2002) Recycled dehydrated lithosphere observed in plume-influenced mid-ocean-ridge basalt. Nature 420:385–389

Doucet S, Weis D, Scoates JS, Nicolaysen K, Frey FA, Giret A (2002) The depleted mantle component in Kerguelen Archipelago basalts: petrogenesis of tholeiitic-transitional basalts from the Loranchet Peninsula. J Petrol 43:1341–1366

Doucet S, Scoates JS, Weis D, Giret A (2005) Constraining the components of the Kerguelen mantle plume: a high-precision Hf-Pb-Sr-Nd isotopic study of picrites and high-MgO basalts from the Kerguelen Archipelago. Geochem Geophys Geosys. doi:10.1029/2002GC000482

Duncan RA (2002) A time frame for construction of the Kerguelen Plateau and Broken Ridge. J Petrol 43:1109–1119

Ellis DJ, Thompson AB (1986) Subsolidus and partial melting reactions in the quartz-excess $CaO + MgO + Al_2O_3 + SiO_2 + H_2O$ system under water-excess and water-deficient conditions to 10 kbar: some implications for the origin of peraluminous melts from mafic rocks. J Petrol 27:91–121

Ford CE (1978) Platinum-iron alloy sample containers for melting experiments on iron bearing rocks, minerals, and related systems. Min Mag 42:271–275

Freise M, Holtz F, Koepke J, Scoates JS, Leyrit H (2003) Experimental constraints on the storage conditions of phonolites from the Kerguelen Archipelago. Contrib Mineral Petrol 145:659–672

Frey FA, Coffin MF, Wallace PJ, Weis D, Zhao X, Wise SW Jr, Wähnert V, Teagle DAH, Saccocia PJ, Reusch DN, Pringle MS, Nicolaysen K, Neal CR, Müller RD, Moore CL, Mahoney JJ, Keszthelyi L, Inokuchi H, Duncan RA, Delius H, Damuth JE, Damasceno D, Coxall HK, Borre MK, Boehm F, Barling J, Arndt NT, Antretter M (2000a) Origin and evolution of a submarine large igneous province: the Kerguelen Plateau and Broken Ridge, southern Indian Ocean. Earth Planet Sci Lett 176:73–89

Frey FA, Weis D, Yang HJ, Nicolaysen K, Leyrit H, Giret A (2000b) Temporal geochemical trends in Kerguelen Archipelago basalts: evidence for decreasing magma supply from the Kerguelen Plume. Chem Geol 164:61–80

Gaetani GA, Grove TL, Bryan WB (1993) The influence of water on the petrogenesis of subduction-related igneous rocks. Nature 365:332–335

Gaillard F, Scaillet B, Pichavant M (2002) Kinetics of iron oxydation-reduction in hydrous silicic melts. Am Mineral 87:829–837

Gardien V, Thompson AB, Grujic G, Ulmer P (1995) Experimental melting of biotite + plagioclase + quartz + muscovite assemblages and implications for crustal melting. J Geophys Res 100:15581–15591

Gautier I, Weis D, Mennessier JP, Vidal P, Giret A, Loubet M (1990) Petrology and geochemistry of the Kerguelen Archipelago basalts: evolution of the mantle sources from ridge to intraplate position. Earth Planet Sci Lett 100:59–76

Ghiorso MS (1997) Thermodynamic models of igneous processes. Ann Rev Earth Planet Sci 25:221–241

Ghiorso MS, Sack RO (1995) Chemical mass-transfer in magmatic processes.4. A revised and internally consistent thermodynamic model for the interpolation and extrapolation of liquid–solid equilibria in magmatic systems at elevated temperatures and pressures. Contrib Mineral Petrol 119:197–212

Grove TL, Bryan WB (1983) Fractionation of pyroxene-phyric MORB at low pressure: an experimental study. Contrib Mineral Petrol 84:293–309

Grove TL, Elkins-Tanton LT, Parman SW, Chatterjee N, Müntener O, Gaetani GA (2003) Fractional crystallisation and mantle-melting controls on calc-alkaline differentiation trends. Contrib Mineral Petrol 145:515–533

Helz RT (1973) Phase relations of basalt in their melting ranges at $P_{H_2O} = 5$ kb as a function of oxygen fugacity. J Petrol 14:249–302

Helz RT (1976) Phase relations of basalt in their melting ranges at $P_{H_2O} = 5$ kb. Part II: melt compositions. J Petrol 17:139–193

Holloway JR, Burnham CW (1972) Melting relations of basalt with equilibrium water pressure less than total pressure. J Petrol 13:1–30

Holtz F, Behrens H, Dingwell DB, Johannes W (1995) H_2O solubility in haplogranitic melts; compositional, pressure, and temperature dependence. Am Mineral 80:94–108

Hoover JD, Irvine TN (1977) Liquidus relations and Mg–Fe partitioning on part of the system Mg_2SiO_4–Fe_2SiO_4–$CaMgSi_2O_6$–$CaFeSi_2O_6$–$KAlSi_3O_8$–SiO_2, vol 77. Carnegie Institute of Washington Yearbook, pp 774–784

Hunt JB, Hill PG (2001) Tephrological implications of beam size-sample-size effects in electron microprobe analysis of glass shards. J Quat Sci 16:105–117

Ingle S, Weis D, Doucet S, Mattielli N (2003) Hf isotope constraints on mantle sources and shallow-level contaminants during Kerguelen hot spot activity since ~120 Ma. Geochem Geophys Geosys. doi:10.1029/2004GC000806

Johnson MC, Anderson AT Jr, Rutherford MJ (1994) Pre-eruptive volatile contents of magmas. In: Carroll MR, Holloway JR (eds) Volatiles in Magmas, vol 30. Mineralogical Society of America, Washington, DC, pp 281–330

Klimm K, Holtz F, Johannes W, King PL (2003) Fractionation of metaluminous A-type granites: an experimental study of the Wangrah Suite, Lachlan Fold Belt, Australia. Precam Res 124:327–341

Koepke J (1997) Analyse von wasserhaltigen silikatischen Gläsern mit der Mikrosonde: Wassergehalte und Alkaliverluste. Beih J Mineral 9:200

Koepke J, Johannes W, Becker A (1996) Determination of crystal/melt fractions with the help of BSE-pictures and image analysis. Terra Nova 8:36

Korenaga J (2005) Why did not the Ontong Java Plateau form subaerially. Earth Planet Sci Lett 234:385–399

Kress VC, Carmichael SE (1991) The compressibility of silicate liquidus containing Fe_2O_3 and the effect of composition, temperature, oxygen fugacity and pressure on their redox states. Contrib Mineral Petrol 108:82–92

Leake BE, Woolley AR, Arps CES, Birch WD, Gilbert MC, Grice JD, Hawthorne FC, Kato A, Kisch HJ, Krivovichev VG, Linthout K, Laird J, Mandarino J, Maresch WV, Nickel EH, Rock NMS, Schumacher JS, Smith DC, Stephenson NCN, Ungaretti L, Whittaker EJW, Youzhi G (1997) Nomenclature of amphiboles. Report of the Subcommittee on Amphiboles of the International Mineralogical Association Commission on new minerals and mineral names. Eur J Min 9:623–651

Martel C, Pichavant M, Bourdier JL, Traineau H, Holtz F, Scaillet B (1998) Magma storage conditions and control of eruption regime in silicic volcanoes; experimental evidence from Mt. Pelee. Earth Planet Sci Lett 156:89–99

Miyashiro A (1974) Volcanic rock series in island arcs and active continental margins. Am J Sci 274:321–355

Morimoto N, Fabries J, Ferguson AK, Ginzburg IV, Ross M, Seifert FA, Zussman J, Aoki K, Gottardi G (1988) Nomenclature of pyroxenes. Am Mineral 73:1123–1133

Nafziger RH, Ulmer GC, Woermann E (1971) Gaseous buffering at one atmosphere. In: Ulmer GC (ed) Research techniques for high pressure and high temperature. Springer, Berlin

Naumann TR, Geist DJ (1999) Generation of alkalic basalt by crystal fractionation of tholeiitic magma. Geology 27:423–426

Nicolaysen K, Frey FA, Hodges KV, Weis D, Giret A (2000) $^{40}Ar/^{39}Ar$ geochronology of flood basalts from the Kerguelen Archipelago, southern Indian Ocean: implications for Cenozonic eruption rates of the Kerguelen plume. Earth Planet Sci Lett 174:313–328

Ohlhorst S, Behrens H, Holtz F (2001) Compositional effect of molar absorptivities of near-infrared OH- and H_2O bands in rhyolitic to basaltic glasses. Chem Geol 174:5–20

Pitzer KS, Sterner SM (1994) Equation of state valid continuously from zero to extreme pressures for H_2O and CO_2. J Chem Phys 102:3111–3116

Putirka K, Johnson M, Kinzler R, Longhi J, Walker D (1996) Thermobarometry of mafic igneous rocks based on clinopyroxene-liquid equilibria, 0–30 kbar. Contrib Mineral Petrol 123:92–108

Ratajeski K, Sisson TW (1999) Loss of iron to gold capsules in rock-melting experiments. Am Mineral 84:1521–1527

Robie RA, Hemingway BS, Fischer JR (1978) Thermodynamic properties of minerals and related subtances at 298.15 K and 1 bar (105 Pascals) pressure and at higher temperature. Geol Surv Bull 1452:456

Roux J, Lefèvre A (1992) A fast-quench device for internally heated pressure vessels. Eur J Min 4:279–281

Ryabchikov ID, Ntaflos T, Büchl A, Solovova IP (2001) Subalkaline picrobasalts and plateau basalts from the Putorana Plateau (Siberian Continental Flood Basalt Province): 1. mineral compositions and geochemistry of major and trace elements. Geochem Int 39:415–431

Ryabchikov ID, Solovova IP, Kogarko LN, Bray GP, Ntaflos T, Simakin SG (2002) Thermodynamic parameters of generation of meymechites and alkaline picrites in the Maimecha-Kotui Province: evidence from melt inclusions. Geochem Int 40:1031–1041

Scaillet B, McDonald R (2003) Experimental constraints on the relationships between peralkaline rhyolites of the Kenya Rift Valley. J Petrol 44:1867–1894

Scaillet B, Pichavant M, Roux J (1995) Experimental crystallisation of leucogranite magmas. J Petrol 36:663–705

Schwab RG, Küstner D (1981) The equilibrium fugacities of important oxygen buffers in technology and petrology. Neu Jahrb Min 140:111–142

Scoates JS, Cascio ML, Weis D, Lindsley D (2006) Experimental constraints on the origin and evolution of mildly alkalic basalts from the Kerguelen Archipelago, Southeast Indian Ocean. Contrib Mineral Petrol 151:582–599

Shaw HR, Wones DR (1964) Fugacity coefficients for hydrogen gas between 0°C and 1,000°C for pressures to 3,000 atm. Am J Sci 262:918–929

Sisson TW, Grove TL (1993) Experimetal investigations of the role of H_2O in calc-alkaline differentiation and subduction zone magmatism. Contrib Mineral Petrol 113:143–166

Thy P, Lesher CE, Fram MS (1998) Low pressure experimental constraints on the evolution of basaltic lavas from Site 917, Southeast Greenland continental margin. In: Proceedings of the Oceans Drilling Program (Scientific results), vol 121, pp 359–372

Toplis MJ (2005) The thermodynamics of iron and magnesium partitioning between olivine and liquid: criteria for assessing and predicting equilibrium in natural and experimental systems. Contrib Mineral Petrol 149:22–39

Toplis MJ, Carroll MR (1995) An experimental study of the influence of oxygen fugacity on Fe–Ti oxide stability, phase relations, and mineral-melt equilibra in ferro-basaltic systems. J Petrol 36:1137–1170

Toplis MJ, Carroll MR (1996) Differentiation of ferro-basaltic magmas under conditions open and closed to oxygen: implications for the Skaergaard intrusion and other natural systems. J Petrol 37:837–858

Wallace PJ (2002) Volatiles in submarine basaltic glasses from the Northern Kerguelen Plateau (ODP Site 1140): Implications for source region compositions, magmatic processes, and plateau subsidence. J Petrol 43:1311–1326

Weis D, Frey FA (2002) Submarine basalts of the northern Kerguelen Plateau: interaction between the Kerguelen Plume and the southeast Indian ridge revealed at ODP Site 1140. J Petrol 43:1287–1309

Weis D, Bassias Y, Gautier I, Mennessier JP (1989) Dupal anomaly in existence 115 Ma ago: evidence from isotopic study of the Kerguelen Plateau (South Indian Ocean). Geochim Cosmochim Acta 53:2125–2131

Weis D, Frey FA, Leyrit H, Gautier I (1993) Kerguelen Archipelago revisited: geochemical and isotopic study of the Southeast Province lavas. Earth Planet Sci Lett 118:101–119

Weis D, Frey FA, Giret A, Cantagrel JM (1998) Geochemical characteristics of the youngest volcano (Mount Ross) in the Kerguelen Archipelago: Inferences for magma flux, lithosphere assimilation and composition of the Kerguelen plume. J Petrol 39:973–994

Weis D, Frey FA, Schlich R, Schaming M, Montigny R, Damasceno D, Matthielli N, Nicolaysen KE, Scoates JS (2002) Trace of the Kerguelen mantle plume: evidence from seamounts between the Kerguelen Archipelago and Heard Island, Indian Ocean. Geochem Geophys Geosys. doi:10.1029/2001GC000251

Yang HJ, Frey FA, Weis D, Giret A, Pyle D, Michon G (1998) Petrogenesis of the flood basalts forming the northern Kerguelen Archipelago: implications for the Kerguelen plume. J Petrol 39:711–748